



HAL
open science

Uranium speciation in a chalky soil

Simon Bayle, Maria Rosa Beccia, Christophe Moulin, Pier Lorenzo Solari,
Christophe den Auwer, Pierre Crançon

► **To cite this version:**

Simon Bayle, Maria Rosa Beccia, Christophe Moulin, Pier Lorenzo Solari, Christophe den Auwer, et al.. Uranium speciation in a chalky soil. Environmental Science and Technology, 2023. hal-04361004

HAL Id: hal-04361004

<https://hal.science/hal-04361004>

Submitted on 22 Dec 2023

HAL is a multi-disciplinary open access archive for the deposit and dissemination of scientific research documents, whether they are published or not. The documents may come from teaching and research institutions in France or abroad, or from public or private research centers.

L'archive ouverte pluridisciplinaire **HAL**, est destinée au dépôt et à la diffusion de documents scientifiques de niveau recherche, publiés ou non, émanant des établissements d'enseignement et de recherche français ou étrangers, des laboratoires publics ou privés.

Uranium speciation in a chalky soil

Simon Bayle^{1,2,3} (ORCID 0000-0003-3851-5459), Maria Rosa Beccia¹ (ORCID 0000-0001-5397-9759), Christophe Moulin^{3,4}, Pier Lorenzo Solari^{2*}, Christophe Den Auwer^{1*} (ORCID 0000-0003-2880-0280), Pierre Crançon^{3*} (ORCID 0000-0002-9207-2663)

1 Université Côte d'Azur, CNRS, ICN, 06108 Nice, France

2 Synchrotron SOLEIL, L'Orme des Merisiers, Départementale 128, F-91190, Saint-Aubin, France

3 CEA, DAM, DIF, F-91297 Arpajon, France.

4 Secrétariat Général à la Défense et Sécurité Nationale, F-75007, Paris, France

Pier Lorenzo Solari, pier-lorenzo.solari@synchrotron-soleil.fr

Christophe Den Auwer, christophe.denauwer@univ-cotedazur.fr

Pierre Crançon, pierre.crancon@cea.fr

Abstract

In this article, the speciation and behavior of anthropogenic metallic uranium deposited on natural soil is approached by combining EXAFS (Extended X-ray Absorption Fine Structure), and TRLFS (Time-Resolved Laser-induced Fluorescence Spectroscopy). First, uranium (uranyl) speciation was determined along the vertical profile of the soil and bedrock by linear combination fitting of the EXAFS spectra. It shows that uranium migration is strongly limited by the sorption reaction onto soil and rock constituents, mainly mineral carbonates and organic matter.

Second, uranium sorption isotherms were established for calcite, chalk and chalky soil materials along with EXAFS and TRLFS analysis. The presence of at least two adsorption complexes of uranyl onto carbonate materials (calcite) could be inferred from TRLFS. The first uranyl tricarbonato complex has a liebigite type structure and is dominant for low loads on the carbonate surface (< 10 mgU/kg(rock)). The second uranyl complex is incorporated into the calcite for intermediate (~ 10 to 100 mgU/kg(rock)) to high (high: > 100 mgU/kg(rock)) loads.

Finally, the presence of uranium-humic substance complex in subsurface soil materials was underlined in the EXAFS analysis by the occurrence of both monodentate and bidentate carboxylate (or/and carbonate) functions, and confirmed by sorption isotherms in the presence of humic acid. This observation is of particular interest since humic substances may be mobilized from soil, potentially enhancing uranium migration under colloidal form.

Key words

Uranium, speciation, X-ray absorption spectroscopy, migration, carbonates.

Synopsis

We explore the speciation and behavior of anthropogenic metallic uranium deposited on natural soil by a multi-faceted technical platform which combines EXAFS (Extended X-ray Absorption Fine Structure) and TRLFS (Time-Resolved Laser-induced Fluorescence Spectroscopy).

Introduction

Uranium is naturally present at various levels in the earth's crust, but can be transformed by human activities such as mining, agriculture (phosphate fertilizers) and military industries or conflicts (Kosovo, Iraq).¹⁻⁶ Therefore, uranium, transformed into various chemical and physical forms, may be concentrated on a local level in the environment. Generally speaking, this is referred to under the so-called TNORM (Transformed Naturally Occurring Radioactive Material) denomination.

Many studies have examined the health effects, corrosion, speciation and mobility of uranium in soil and subsurface.^{3,5-14} The behavior of uranium in subsurface environments is strongly related to its geochemical background, which is also driven by water-rock interactions.¹⁵ Under oxic and suboxic conditions, the oxo form of uranium (named U(VI) in the following, and usually called uranyl) is mostly present in subsurface solid materials by sorption, coprecipitation or complexation mechanisms.^{1,12,16-22} But reduction to U(IV) may also occur in geochemical or biochemical reducing conditions.²³ Nevertheless, speciation in the presence of strong complexing ligands present naturally in the environment like carbonates²⁴⁻²⁶ or humic substances,^{1,3,8,27-32} redox processes,³³⁻³⁵ as well as sorption to rapid colloidal vehicles,^{31,36-39} may be responsible for a potential long-range migration of uranium in the environment. This latter process may lead to a significant proportion of uranium in surface water⁴⁰ or groundwater^{26,41} transported as suspended particles or colloids.^{1,42,43} On the other hand, the migration of uranium in carbonate-rich environments leads to the formation of stable uranyl-calcium-tricarbonate complexes that decrease the uranyl adsorption onto natural solid materials, thus potentially enhancing its mobility in soil, sediments and groundwater.^{24,25,43-47}

In the more specific and restricted framework of military applications, the use of uranium munitions on the battlefields of Kosovo or Iraq has led to uranium concentration in soils above levels classically found in geological materials.^{4,48-50} This has also been detected in technical firing ranges.^{32,50-52} In the case of the war in Kosovo,^{4,51,53-55} these were initially deposited as large metallic fragments and pellets, small shells, and particles.^{3,9-11,22,56,57} In these conditions, oxidation over time of the initial U(0) deposits in soil most often leads to mixed U(IV)/U(VI) oxides in various forms and proportions.^{3,22,58} At the same time, in oxic conditions, leaching, caused by rainfall of metallic U fragments further altered in UO₂(s), then produces highly soluble uranyl oxyhydroxide such as metaschoepite ((UO₂)₈O₂(OH)₁₂•10(H₂O)),^{3,59-64} which might then migrate through the soil toward the surface of shallow aquifers.⁶¹⁻⁶⁵

This short review underlines the need for speciation data in the open field when U(0) fragments have been deposited for a long time (more than 10 years). Nevertheless, speciation data is required for determination and modeling of migration mechanisms, such as retention on the immobile phases or complexation with mobile ligands such as humic substances. In this paper, we propose to describe the geochemical behavior of metallic uranium deposited in a natural carbonate rendosol (or rendzina, following U.S. classification) in a former military site. These uranium materials had subsequently undergone natural alteration (essentially linked to weathering) for several decades under oxic

conditions.^{45,66} They had also undergone migration processes in the soil, going deeper in the subsurface through Cenomanian chalk substrate. We combine here analytical chemistry (ICP-MS), X-ray Absorption Fine Structure spectroscopy (XAFS) at the U L edge and Time Resolved Laser Fluorescence Spectroscopy (TRLFS) in order to generate a full picture of the migration mechanisms in the natural soil.

Materials and Methods

1. Study site location, geological and geochemical settings

The migration of uranium in deep soil horizons was investigated in a localized deposit of dispersed metallic uranium U(0) nuggets and particles on the surface of a carbonate rendosol (*i.e.* rendzina), developed on a chalk substrate from the Upper Cretaceous (\approx 100 to 65 million years ago). Details about the study site and the geological and geochemical settings are given elsewhere, as well as preliminary results on the U distribution and aqueous and colloidal speciation in the subsurface and aquatic environment.^{45,66–75} The vegetation on site is a dry grasslands developed on thin chalky rendzina and calcisols more or less cryoturbated, with low organic carbon content (Total Organic Carbon mass content typically lower than 5%). Table S1 of SI summarizes the essential information about the mineralogical and organic composition of the soil and the chalk substrate at the study site, and their evolution along a vertical soil profile. Soils and colluviums are characterized by a larger non-carbonate fraction as opposed to the chalk units. The soil exhibits three main horizons (Figure 1). The topsoil layer is a thin (thickness \sim 10 cm) Aca horizon, poorly developed, that exhibits a porous and granular structure characterized by an organic matter content of about 5 mass.%. The mineral content is more than 60% of calcium carbonates (mainly calcite, with traces of dolomite), supplemented by a non-carbonate fraction composed of \sim 35% of silicates and aluminosilicates such as silica, kaolinite, feldspar and micas, and about 3% iron oxy-hydroxide.^{45,69,71} The second soil horizon is a transitional silty-clay altered (Sca type) and extends from \sim 10 to 60-70 cm deep, and is composed of chalk (86%), organic matter (\sim 5%) and of iron oxides. The bedrock is constituted by a cryoturbated chalky substrate that contains more than 95% calcite, less than 5% of aluminosilicates, and an organic matter content about 25 times lower (\sim 0.2 %) than that measured in the topsoil layer. A surface soil (0-20 cm) and a deeper host rock (Campanian chalk, 1-2 m) were collected within the site limits but outside the historical uranium deposits area and are referred to hereinafter as Chalky Soil and Chalk respectively. Soil and subsoil samples for the determination of the uranium vertical migration profile were collected every 10 cm in a trench dug in the deposits area of the former military site, at increasing depth from the surface to 2 m depth.⁷⁶

In order to take into account the heterogeneity of uranium distribution in deposit and soil materials, the samples were taken over a horizontal width of 20 cm, crushed, dried, and then homogenized by quartering before being put into 500 ml vials calibrated for gamma spectrometry. Raw samples were

air-dried, prescreened by sieving at 5 mm to remove the largest gravel particles and other fragments, crushed gently, and again sieved to a particle size of < 200 μm prior to physicochemical characterizations and adsorption experiments.

2. Uranium model materials

Altered uranium pellets from the initial deposit. Altered U nuggets were picked manually from the soil's surface inside the field site, then gently washed with distilled water to remove soil particles. Visually, nuggets can be divided into two main categories: dark-colored and yellowish-colored (Figure 2a).

Uranyl-oxo-hydroxide reference (Metaschoepite). Metaschoepite reference sample was synthesized following the method proposed by Bruno et al.,⁷⁷ by dissolving uranyl acetate ($\text{UO}_2(\text{H}_4\text{C}_2\text{O}_2)_2$) under argon atmosphere, in a 5% perchloric acid solution and using degassed purified water. Then, the pH was adjusted to 7 using a 0.1 M NaOH solution. The precipitate formed after a few minutes, was isolated after solution filtration and extensively rinsed using degassed purified water. The composition and structure of metaschoepite was then confirmed by X-ray diffraction (data not shown).

U-HA sample. Humic acids Sigma-AldrichTM in solid form were dissolved in distilled water at atmospheric equilibrium ($p\text{CO}_2 \approx 10^{-3.5}$ atm) to obtain a concentration of $[\text{HA}] = 5 \text{ g.L}^{-1}$, which was continuously stirred for a period of 24 h. U(VI) was added to 10 mL of the humic acid solution (no undissolved HA was visible) from a stock solution (PlasmaCAL, Standard for ICP, SCP Science, 10000 $\mu\text{g/mL}$ in 4% HNO_3) to obtain a final U concentration of $[\text{U}] = 10^{-3} \text{ mol.L}^{-1}$. Once U was added to the humic acid solution, the pH was adjusted to 7.5-8 using 0.1 M NaOH solution.

U-triscarbonate sample. The uranyl triscarbonate sample ($\text{UO}_2(\text{CO}_3)_3^{4-}$) was prepared by mixing a uranyl stock solution (PlasmaCAL, Standard for ICP, SCP Science, 10000 $\mu\text{g/mL}$ in 4% HNO_3) in the presence of an excess of carbonate at 0.5 mol.L^{-1} obtained by dissolving Na_2CO_3 . The final U concentration was equal to $4.2 \cdot 10^{-2} \text{ mol.L}^{-1}$, and the pH was adjusted to 7.5.

Uranyl-calcium tricarbonat sample: mineral Liebigite reference sample ($\text{Ca}_2[\text{UO}_2(\text{CO}_3)_3] \cdot 11\text{H}_2\text{O}$) was obtained from the mineralogy collection of the Musée National d'Histoire Naturelle (MNHN), Paris, France.

3. Experimental sorption isotherms

Batch sorption experiments. Adsorption isotherms of U(VI) were determined onto synthetic and natural carbonate substrates : purified calcite in the presence and in the absence of humic acid, natural chalk and chalky soil from the study site.

Batch experiments conducted at 25 °C in an open and oxic atmosphere. All solutions and suspensions were prepared with deionized Milli-Q 18 M Ω cm (MilliporeTM) water. Purified calcite and Humic Acid were from Sigma-AldrichTM (detailed properties are given elsewhere^{78,79}). The specific surface

area for carbonate materials (calcite, chalk and chalky soil) were determined by BET method (see Table S2 of SI). Solid sorbents (calcite, chalky soil, chalk) were put in suspension with distilled water, in order to obtain a mass out of volume ratio close to 100 g.L⁻¹. After 2 weeks of stirring and the solution being considered at equilibrium, U(VI) was added in the reactor with an initial concentration ranging from ~ 1 to 1 × 10⁶ µg. L⁻¹, in solutions prepared by dilution from parent stock solution of uranyl nitrate (1000ppm, Fluka™) with deionized water. After the addition of U, the pH of the suspension was adjusted to 7.3 with HCl or NaOH, if necessary. Reactors consisted either of a closed 50 ml PTFE reaction vessel (for U adsorption on calcite), or on a 2 part Pyrex® glass reaction vessel (Ace- Glass Inc, NJ, USA) containing a working volume of 1 L (for U adsorption on chalky soil and chalk), and constantly shaken during the duration of the experiment (1 week). The pH of the suspensions was recorded every 3 days using solid polymer open junction Xerolyt electrodes (Mettler-Toledo, France). The reacted suspensions were sampled after one week of equilibrium at room temperature (25°C). The samples were quickly filtered and acidified with 2% HNO₃ before the analysis. Concentration of U was measured by ICP-MS (Perkin Elmer ICP-MS Elan DRC-e) with expanded uncertainty established at a level of confidence of 95%.

Sorption Isotherms modelling. Experimental sorption isotherms data were modelled with three different functions: Kd, Freundlich and Langmuir isotherms (see details in SI paragraph 2.), in order to determinate sorbent sorption capacity from parameter estimation.⁸⁰⁻⁸³

4. XAFS main settings

All XAFS (X-ray Absorption Fine Structure) analyses were performed on the MARS beamline of SOLEIL synchrotron (Saint-Aubin, France).^{84,85} The beamline optics consist essentially of a water-cooled double-crystal monochromator (FMB Oxford), which is used for selecting the incident energy of the X-ray beam and for horizontal focusing, and two large water-cooled reflecting mirrors (IRELEC/SESO) that are used for high-energy rejection (the harmonic part) and vertical collimation and focusing of the X-ray beam. All measurements were taken in fluorescence mode using a 13-element high purity germanium detector (ORTEC, electronics XIA -XMA).

EXAFS data acquisition and processing. U L_{II} edge (20 948 eV) was probed to analyze the L_{β1} fluorescence line (17 220 eV) in the natural soil samples. This choice is justified by the fact that a strong K edge fluorescence line of strontium at 14165 eV is present close to the main fluorescence line of U at the L_{III} edge (13 614 eV) due to the high concentrations of Sr in the carbonate materials of the study site. Consequently, beam energy calibration was performed at the molybdenum K edge (20 000 eV).

All EXAFS data processing was performed using the ATHENA code.⁸⁶ The E₀ energy was identified at the maximum of the first derivative around absorption edge. Fourier transform (FT) was performed with a Hanning window. Fourier transform with k² weighting was performed between 3.5 and 12 Å⁻¹

for each reference sample. Fittings of the references were performed in R space between 1 and 5 Å using the ARTEMIS code (version DEMETER 0.9.25).⁸⁶ The same global amplitude factor S_0^2 and the same energy threshold correction factor ΔE_0 were used for every path of the fits. The agreement factor r (%) and the quality factor ($QF = \chi_{red}^2$) of the fits were provided directly by DEMETER. Partial structural models were used for the pure U phases to calculate phases and amplitudes using the FEFF6 simulation code integrated in DEMETER.

EXAFS data treatments of soil samples by Linear Combination Fitting (LCF). EXAFS spectra of soil samples from the vertical U migration profile were analyzed by Linear Combination Fitting in a three component-mixing model, using the EXAFS spectra of U-triscarbonate, metaschoepite and U-AH complex as references, respectively. LCF was performed with a mean square routine on EXAFS spectra between 3.5 and 10 Å⁻¹ in k space. Hence, the amplitude of each reference compound in the composition of each soil sample was determined. The sum of the weight of the combination was left free to evolve.

Uranium samples preparation. All soil samples were finely crushed in fine powder with an agate stone pestle. A total mass of 5 mg of either U nugget from the polluted soil (nugget #2) or reference synthetic metaschoepite was accordingly crushed then mixed with about 195 mg of polyethylene to limit fluorescence reabsorption during XAFS analysis.

5. Time-Resolved Laser Fluorescence Spectroscopy main settings

Time-resolved fluorescence spectra of uranyl species in the solid phase were collected at room temperature using a FP920 spectrofluorometer with embedded ICCD (Intensified Charge Couple Device) camera (Edinburgh InstrumentsTM) cooled at -20°C by Peltier effect and coupled to a Nd-YAG (QuantelTM Surelite) laser source delivering an initial beam of 10 mJ energy at 1064 nm (~1.2 eV), with a 10 Hz pulse frequency. For fluorescence spectroscopy, the excitation beam was set to 355 nm (third harmonic, ~3.5 eV). The sample holder and the ICDD camera were oriented respectively at 45° and 90° from the incident axis to avoid direct laser beam transmission. Data acquisition and pre-processing was performed by F900 software (Edinburgh InstrumentsTM). Data post-processing (baseline determination and spectra deconvolution by Gauss functions) is performed using Origin 2002 Pro (Origin LabTM).

Results

1. Profile of uranium concentration in soil

The concentration of U in a soil profile was determined on a series of discrete samples with 10-cm increments from the surface to a depth of 2 m in a trench dug in the site. Total U content was

determined from ICP-MS analysis after complete solubilization of soil and rock materials by hydrofluoric acid. Details of the analysis results are reported in SI, Table S1 and Figure S1. Figure 1 shows the profile of the soil U content compared to a picture and a brief description of the soil's structure. The blue dotted lines represent the mean natural U concentration in the geochemical background of the Campanian chalks (and surrounding soils) (close to 1 ppm) as determined outside the site.⁴⁵ The highest U content is found in the topsoil layer, corresponding to the initial surface deposit. Then, its content in the soil decreases rapidly according to depth, from 0 to 50 cm, constitutively with soil organic matter content (Table S1 of SI). Below, the U content decreases asymptotically down to a depth of 2 m, where there is a predominant amount of carbonate minerals in the chalk materials. Throughout the soil's surface, the U deposit appears to be essentially constituted by fine particles of alteration products (lower than ~50 μm in size), as confirmed by electron microscope imaging (Figure S2 of SI). The continuous decrease of U content according to depth corresponds to a migration front that extends beyond 250 cm deep, where U content in chalk remains four times higher than the geochemical background in surrounding rocks. The migration of U towards deeper chalk horizons thus appears to be limited by retention onto geological materials. There is a positive correlation between U and organic matter contents throughout the vertical profile (Figure S1 of SI). This being said, the influence of the chemical composition of the soil matrix on the U speciation and retention, thus its migration regime, needs to be demonstrated.

2. Batch sorption experiments

Experimental sorption isotherms of U onto pure calcite are reported in Figure 3 (see Table S3 of SI for experimental conditions), and compared to data from the bibliography.⁸⁷⁻⁸⁹ All these sorption isotherms use calcite materials from various origins, with various surface properties, solid/liquid ratios (varying from 5 to 100 g.L^{-1}) and pH conditions (from 7.0 to 9.1). Nevertheless, isotherm data are globally consistent. The lower the solid/liquid ratio and the calcite grain size, the higher the specific surface area and the sorption of U are. The U affinity for calcite surface is mild, with distribution coefficient K_d (see Table S4 of SI) ranging from 3 to 21 L.kg^{-1} . Sorption patterns on calcite are mainly non-linear, exhibiting typical Freundlich (at low adsorbate concentrations) or Langmuir patterns (for higher adsorbate concentration, and when experimental conditions are closer to critical U concentrations in adsorbate regarding either sorbent surface saturation or U solid phase solubility) with significant correlation coefficients higher than 0.90. The n values between 0.6 and 0.9 reported for the Freundlich isotherms suggest that the adsorption process depends more or less on the surface coverage of the adsorbent and is not strictly proportional to the concentration of the adsorbate in solution. As a consequence, the uranyl adsorption reaction has a global stoichiometry less than 1.⁸² Maximal adsorption capacity of the sorbent q_m estimated from Langmuir function fitting are typically ranging from 0.02 to 6 $\mu\text{mol.m}^{-2}$ consistent with previous observation on pure synthetic calcite.^{88,90}

The experimental sorption isotherms of U onto chalk are also reported in Figure 3, and compared to data from Géhin *et al.* obtained on the same materials under identical conditions.⁹¹ U sorption isotherms on chalk are consistent and close in form and properties to the sorption isotherms for uranyl on calcite. U affinity for chalk is lower than that of calcite, with distribution coefficient K_d ranging from 0.3 to 10 L.kg⁻¹. Comparable to calcite, U sorption patterns on chalk are mainly non-linear. The n values reported for Freundlich isotherms are close to 0.3 - 0.8, suggesting (as for pure calcite) a multiple speciation and sorption mechanism for U on chalk, dependent on adsorbate concentration in solution, with a global stoichiometry for the sorption reaction lower than 1. Maximal adsorption capacity q_m estimated for chalk from the Langmuir equation are lower than that of calcite, and typically range from 0.01 to 0.1 $\mu\text{mol.m}^{-2}$ (Table S4 of SI).

Finally, sorption isotherms for U on chalky soil are consistent with the sorption isotherms for U on pure calcite and chalk, but with a slightly higher affinity (K_d close to 20 L.kg⁻¹, see Table S4 in SI). Comparable to those for calcite and chalk, U sorption patterns on chalky soil are non-linear, with n values reported for Freundlich isotherms close to 0.3-1.0. Maximal adsorption capacities q_m estimated for chalky soil from the Langmuir equation (about 0.1 - 0.7 $\mu\text{mol.m}^{-2}$) are slightly higher than those estimated for chalk. Since the composition of chalky soil mixes calcite (~ 60%) with secondary silicates, oxides and organic phases (~ 10% kaolinite, ~ 10% clays and feldspars, ~ 15% silica, ~ 5% iron and aluminum oxi-hydroxides, ~ 1% organic carbon), this increasing affinity of U for soil materials compared to chalk may be imputed in large part to secondary phases, as classically observed in geological subsurface materials.^{1,18,92,93}

As a complement, the sorption of U onto chalk doped with purified Aldrich humic acid (HA) was studied in batch experiments ([chalk + HA] = 100 g.L⁻¹, with [HA] = 2 mass.%). U affinity for chalk + HA is notably higher than for chalk, with the distribution coefficient estimated K_d close to 26 L.kg⁻¹, and remarkably close to U affinity for the chalky soil. Sorption isotherms for uranyl on chalk+HA and chalky soil are very similar. Thus, complexing organic compounds such as humic acids are likely to play a key role in U retention in soil materials, as already observed by many authors.^{1,94-101}

3. Uranium speciation determination

EXAFS and TRLFS analysis of the source term deposits and uranyl references

Heterogeneously dispersed particles and fragments constitute the initial U deposit on the soil's surface. Larger fragments that range from a few millimeters to a few centimeters in size are hereafter called U nuggets. Two different nuggets of about 2 mm in size (nuggets #1 and #2, Figure 2a), were sampled on the site and are fully oxidized displaying the characteristic dark-yellowish color of uranyl hydrates. Despite a color difference, solid phase composition is found to be rather homogeneous between the two nuggets. Dark-yellowish colored pellet (nugget #1) is found to be very close to schoepite $\alpha\text{-UO}_2(\text{OH})_2$ with low crystallinity. The yellowish-colored altered pellet (nugget #2) is found to be composed of an assemblage of various low-crystallinity uranyl hydrates, mainly represented by

pseudo schoepite ($\text{U(VI)O}_{3+x}\cdot 2\text{H}_2\text{O}$) or metaschoepite ($(\text{UO}_2)_8\text{O}_2(\text{OH})_{12}\cdot 10(\text{H}_2\text{O})$) (X-ray diffraction data, see X-ray diffractogram of Figure 2b). The EXAFS spectra recorded at the U L_{II} edge for nuggets #1 and #2 are given in Figure 2c, together with their Fourier transform (FT, Figure 2d). Spectra of nuggets #1 and #2 are remarkably similar and can be adjusted with structural parameters close to those of metaschoepite (Table S5 of SI): 2 axial O at $1.82 \pm 0.01 \text{ \AA}$, 2.4 ± 0.2 equatorial O at $2.32 \pm 0.1 \text{ \AA}$ and 2.4 ± 0.2 equatorial O at $2.5 \pm 0.1 \text{ \AA}$, and about 3 ± 0.5 distant U at $3.8 \pm 0.15 \text{ \AA}$. This also confirms that U is fully oxidized to oxidation state +VI in these two samples where uranium is present as a mixture of oxyhydroxide complexes. Time Resolved Laser Fluorescence Spectroscopy (TRLFS) spectra for nugget #1 and synthetic metaschoepite are given in Figure S4 of SI, together with respective deconvolution peaks. Table S6 of SI gives corresponding details of spectra and lifetime properties, together with data from the literature about schoepite and metaschoepite.¹⁰² Four major bands can be identified at about 500, 520, 540 and 569 nm that correspond to a fluorescence pattern identified for metaschoepite.¹⁰² Fluorescence lifetime estimated for nugget #1 ($131 \pm 4 \mu\text{s}$) is higher than that estimated for metaschoepite ($50 \pm 5 \mu\text{s}$). The breadth of vibronic bands and the poor resolution of the spectra are consistent with the presence of multi-phase precipitates with various hydration states, resulting in multiple local U environments in the structure of uranyl hydrates, as has been cited by many authors.^{88,90,103}

A uranyl - humic acid complex in solution (named U-HA) was also prepared as a model of uranyl complexation by an excess of HA. The corresponding EXAFS spectrum is given in Figure S3 of SI. The spectrum was fitted with 2 axial O at $1.80 \pm 0.01 \text{ \AA}$, and two distinct U-O equatorial contributions with $2.5 \pm 0.1 \text{ \AA}$ O at $2.29 \pm 0.01 \text{ \AA}$ and $3.0 \pm 0.2 \text{ \AA}$ O at $2.44 \pm 0.01 \text{ \AA}$ (see Table S5 of SI). The structural parameters obtained for the U-HA complex are in agreement with data from the literature on uranyl-carboxylate species, which exhibit two equatorial distances.¹⁰⁴⁻¹⁰⁶ However bidentate {COO} groups can either originate from carboxylate or carbonate groups. In the second case, the uranium would be in the ternary complex form $\text{UO}_2(\text{CO}_3)_2\text{HA}^{2-}$ (described by Steudtner *et al.*¹⁰⁷ under similar conditions). However, the present EXAFS data do not show the contribution from a distal oxygen of the carbonate(s), which can be explained by (1) the absence of any carbonate in the equatorial plane of uranyl, (2) by a lack of sensitivity of the fit to the presence of a distal oxygen (in case there is only one, for instance).

Finally, the EXAFS spectra of the uranyl tricarbonate sample, in solution ($\text{UO}_2(\text{CO}_3)_3^{4-}$, named U-carb) recorded at the U L_{III} edge is also given in Figure S3 of SI. The spectrum has been adjusted (see Table S5 of SI) with 2 axial O at $1.82 \pm 0.01 \text{ \AA}$, and 6 equatorial O at $2.45 \pm 0.01 \text{ \AA}$, corresponding to 3 bidentate CO_3^{2-} groups in very good agreement with the atomic environment of uranium in the Liebigite structure reported in the literature.^{90,108,109}

TRLFS analysis of uranium sorbed onto calcite and soil materials.

The normalized fluorescence spectra of uranium sorbed onto calcite, natural chalk and natural chalky soil are given in Figure S5 of SI for an initial dissolved U concentration varying from 1 to 1000 ppm. Spectral properties and fitting parameters for TRLFS spectra are given in Table S6 of SI. Fluorescence spectra for U sorbed onto calcite, chalk and chalky soil are remarkably similar and are observed to change as the U concentration in the overlying solution, and therefore the U loading at the sorbent surface increases. For the lowest dissolved U concentration (1 ppm), the spectrum is centered at 525 nm and is poorly (but clearly) structured. Five relative maxima, corresponding to five major vibronic bands, are identified respectively at 489, 505, 524, 543 and 570 nm. Assuming this spectrum is assigned to a single component, this pattern observed for a longer-lived species is very close to the one observed for natural liebigite (Figure S6 and other published luminescence data given in Table S6 of SI); and also to U(VI)-substituted synthetic calcite and aragonite in a liebigite-like structure.^{90,102,110} This shows that for low U loadings on the carbonate mineral surfaces (including calcite, chalk and chalky soil), U is mainly associated with calcite within a tricarbonat liebigite-type structure, that represents an adsorbed U species,⁹⁰ and will be hereafter called “species 1”. For U concentrations in overlying solution ranging between 10 to 50 ppm, the fluorescence spectra of U sorbed onto chalk samples exhibit at first a slight blue-shift of the main bands. This suggests a change in the interaction between U(VI) and the calcite surface, leading to the formation of another uranyl tricarbonat-like surface species.^{90,111,112} The fluorescence bands of this second U sorbed species (hereafter called “species 2”) can be isolated from any spectrum recorded on chalk or soil samples with intermediate U loading by subtracting bands of species 1 from the raw fluorescence spectrum (Figure S7 of SI). Five relative maxima can be identified in the subtraction residuals, respectively at 488, 498, 517, 539 and 565 nm, that are found to be very close to those of U incorporated in calcite, as defined by Elzinga (see Table S6 of SI).⁹⁰

Then, for higher dissolved U concentrations (essentially above 100 ppm), the fluorescence pattern becomes more unstructured, centered at about 530 nm, and exhibits a clear red-shift with an apparent smoothing of fluorescence maxima. Uranyl hydroxide precipitates are expected at these concentrations, and indeed the spectra shown in Figure S8 of SI for solutions higher than about 100 ppm are composed of at least two components, the main one being consistent with the luminescence spectra of uranyl hydroxide such as schoepite.^{88,102} As in synthetic metaschoepite and nugget #1, the absence of a clear structure in the vibronic bands indicates that the precipitate is probably not a pure phase.¹¹³ It can be noted that in the presence of HA in the soil samples, the precipitation of uranyl hydrates is delayed and is not significantly observed before the soil U content reaches about 500 ppm. By assigning the global fluorescence signal to a triple component system (species 1 + species 2 + schoepite), all of the spectra recorded for U sorption onto calcite, natural chalk and natural chalky soil given in Figure S5 of SI were able to be convoluted by a linear combination of these three components, with regression coefficients generally above 0.99 (see Figure S8 of SI). Deconvolutions were conducted by keeping a constant, for each component spectrum, the band positions, and the peak

widths and relative areas. Deconvolution results clearly outline the dominance of uranyl-carbonate species 1 for low U loadings on the surface of carbonate materials, and of uranyl-carbonate species 2 for high U loading. The red-shift of fluorescence spectra observed for high U concentrations in adsorbate is clearly attributed to the precipitation of uranyl hydrates.

Qualitative approach of the uranium speciation along the vertical soil profile

The XAFS spectra of the soil samples from the study site, from the surface to a depth of 100 cm (at 0, 10, 20, 30, 40, 50, 60, 80 and 100 cm), were recorded at the U L_{II} edge. The XANES portion of the absorption spectrum is a fingerprint of the U oxidation state and environment. In this region, the shoulder observed at ca. 15 eV after the white line maximum is typical of multiple scattering features along the trans-dioxo form of uranyl. XANES spectra (Figure S9 of SI, left) and their first derivative (Figure S9, right) clearly indicate that all the soil samples contain U at formal oxidation state +VI under the form of UO_2^{2+} , and that no significant evolution of the oxidation state can be observed from the surface to the lowest points of the vertical profile.

In order to clarify the speciation and its possible evolution down from the surface, EXAFS analysis was also performed on the same soil samples series. The EXAFS spectra of the soil samples at various depths are presented in Figure 4 together with those of three reference materials: i) the metaschoepite-like weathered U nugget taken from the initial deposits (U-nugget #1), ii) an HA uranyl complex in solution (U-HA), and iii) the tri-carbonate uranyl complex in solution (U-carb). It is apparent that the EXAFS spectrum of the surface sample is qualitatively similar to that of the nugget. Going from the subsurface to deeper soil horizons, the XAFS contribution between 6.5 and 9 \AA^{-1} is significantly modified and tends towards a plateau observable on the U-carb reference spectrum. The signal to noise ratio decreases from subsurface to depth because of the decrease of U quantity in the sample. On the corresponding Fourier transforms (FT) shown in Figure S10 of SI, an evolution of the second contribution of the FT between $R+\Phi = 1.7$ and 2.5 \AA is also clearly visible. This second contribution is associated with the equatorial oxygens of the uranyl oxocation, and the modification of the modulus of the FT suggests a rearrangement of these oxygens. Finally, a U-U contribution in R space at $R+\Phi = 3.8$ \AA is clearly observable in subsurface samples above 20 cm. This U-U contribution, characteristic of a condensed phase (as for the spectra of U-nugget #1, #2), and clearly visible for surface soil samples, decreases with depth and is undistinguishable below 30 cm, as can be seen for the deepest sample of the profile at 100 cm.

Normalized TRLFs spectra for U recorded on the same sample series from the soil vertical profile are given in Figure 5. The fluorescence spectra are broad, poorly resolved, and noisy, despite high U concentration in the soil in the upper layers. These observations suggest a complex multiple-species speciation scheme for U, as well as a significant quenching of the fluorescence signal, and the presence of non-fluorescent species such as U-AH complexes. The maximum fluorescence spectra are observed at ~ 520 nm, consistent with results obtained for U sorption experiments on soil materials. This pattern is very close to the one observed for U sorbed onto calcite, chalk and chalky soil (see

Figures S5 and S6 of SI), and can be attributed to a dominant uranyl tricarbonate species. By subtracting bands of species 1 (liebigite-type structure) from the raw sample spectra, five relative maxima can be mainly identified in residuals at 488, 498, 517, 539 respectively and 565 nm, that correspond to species 2 (U incorporated in calcite, as defined by Elzinga).⁹⁰ All of the spectra recorded along the soil profile were deconvoluted by a combination of three components (species 1 + species 2 + schoepite), together with a wide Gaussian function for representation of the luminescence baseline (Figure S11 of SI). Deconvolution results clearly outline the presence of at least two uranyl-carbonate species that change in proportion with U(VI) loading on the carbonate mineral surface and, consequently, with depth in the soil profile, are consistent with results obtained for U sorption experiments on soil materials. The presence of relictual uranyl hydrates from the initial deposit can be noticed in the topsoil sample, where U concentration is maximal (~ 6500 ppm).

Quantitative approach of uranium speciation using EXAFS Linear Combination Fitting

In order to quantitatively describe the evolution of U speciation along the vertical profile, a linear combination fitting (LCF) procedure was implemented with EXAFS. The LCF procedure considers the three reference materials (components) described above: U-nugget #1, U-HA and U-carb. For each sample, the total number of components was not set to 100% (as it should be) in order to verify that without this constraint, the total percentage does not substantially deviate from 100%. EXAFS linear combination fits are presented in Figure 4, and the respective repartition of the three components obtained from the LCF procedure is represented in Figure 6. Although the 3 components are not significant at all depths (the significance of the selected components as a function of depth is given in Figure S12 of SI with comparative F-tests), a 3-component system was considered for LCF consistency. First, one can observe that all samples along the soil profile are correctly fitted with a combination of the three components mentioned above. Secondly, we see that at the soil's surface (0 cm), U speciation is mainly constituted by uranyl oxyhydroxides (metaschoepite-like) obtained from the alteration of the U nuggets. One can note that only one component (U-nugget #1) is significant for this fit but the model of 3 components was applied for all samples for overall consistency. The corresponding spectrum was fitted according to this assumption and the fit is presented in Figure S13 and Table S7 of SI. Thirdly, from 10 to 60 cm depth, a mixing between the uranyl oxyhydroxides from the deposits and uranium-humic substances complexes can be observed, with a participation of U carbonate in a liebigite-type structure whose contribution ranges from minor (between 10 and 30 cm) to major (between 40 and 60 cm). Finally, below 70 cm depth, the participation of U-carbonate complexes with liebigite-like structure is clearly dominant. And the spectrum of the deepest sample (100 cm) was also fitted according to this assumption (see Figure S13 and Table S7 of SI) showing the consistency of the LCF result.

Discussion

In the soil profile of the study site, uranium is initially deposited as U metal fragments and particles, called “nuggets”. After alteration, the nuggets that were observed have a schoepite-like structure. The total U content decreases sharply, by more than five orders of magnitude from top to bottom of the vertical profile (250 cm). This continuous decrease in depth correlates firstly with the rapid disappearing of particles from the U nuggets from the initial surface deposits, and secondly, with a migration front of U that extends from the soil’s surface to beyond 250 cm deep. Despite a long period of alteration in the soil (several decades), a large part of the U thus remains in the soil, suggesting that: i) its corrosion is strongly kinetically-limited in soils, consistent with observations made by many authors);^{3,52,58,61,114,115} and ii) a large part of U is retained by sorption onto the geological materials. In all the samples along the soil profile, U is fully oxidized and appears as uranyl U(VI) species.

Experimental sorption isotherms of U on calcite, purified natural chalk and chalky soil show that U is moderately retained on carbonate, comparable to silicate minerals such as clays.^{1,18,92} For comparable pH and temperature conditions, lower sorption capacity is observed for chalk compared to calcite. This may be explained by differences in crystal structure for natural calcite in chalk compared to purified calcite, leading to lower surface site density for calcite in chalk (~ 0.01 to 0.1 $\mu\text{mol.m}^{-2}$), than for purified synthetic calcite (~ 1 to 9 $\mu\text{mol.m}^{-2}$).^{87,88} Sorption isotherms on calcite are mainly nonlinear, exhibiting typical Freundlich (at low adsorbate concentrations) or Langmuir patterns (for higher adsorbate concentration). Sorption isotherms and speciation analysis by both EXAFS and TRLS techniques strongly suggests that U sorption onto chalk and chalky soil follows globally the same speciation scheme as observed for U sorbed onto calcite. The role of secondary phases (essentially organic matter) appears to be predominant at low solid/liquid ratios and/or at high U concentration in adsorbate.

U speciation is observed to evolve from surface to bottom, highlighting several phenomena:

- 1) The decrease in the contribution of uranyl metaschoepite, as in the first 10 - 70 cm of soil, as revealed by EXAFS analysis, attributed to residual weathered fragments and particles of U inherited from the initial deposits. This suggests that the vertical migration of U through the soil is partly realized under micro particle forms. This observation is not surprising, since on the one hand, residual U particles are classically identified in surface soils in comparable contexts (firing test ranges, or battlefields from Kosovo and Kuwait conflicts^{9,10,12,38,116}), and on the other hand, vertical migration of particles is known to occur in soils, enhancing the transport of radioactive fallouts through topsoil horizons.¹¹⁷⁻¹²² The speciation of these micro particles could not be studied within the framework of this research because their size (of the order of a few micrometers) is smaller than the lowest size of the synchrotron beam achievable on the MARS beamline.

- 2) The dominant contribution of the uranium-humic substances complex from 10 to about 60 cm suggests that organic matter is one of the principal complexing agents of U during its migration in the first few decimeters. This is confirmed by sorption isotherms onto chalky soil and onto chalk

doped with humic acids which clearly highlights the part taken by humic substances for complexation and immobilization of U in the chalky soil. Nevertheless, these observations are of interest for further investigations on U migration in the subsurface, since humic substances are also known to be easily mobilizable from soils, mobile in soils and aquifers, and can enhance U migration under colloidal form. ^{36-38,42,43,72,123,124}

3) In the first 120 cm of the soil profile, where U content is typically above 10 ppm, the results of EXAFS and TRIFS speciation analysis and interpretations from sorption isotherms are in agreement. The TRIFS analysis indicates a double speciation of U onto carbonate minerals, revealing the presence of at least two complexes for adsorbed U, that change proportion with U loading with a slight rearrangement of oxygen equatorial coordination, consistent with previous interpretations from other authors.¹²⁵⁻¹²⁷ For low U loading on the calcite surface, a bidentate uranyl tricarbonate complex with a liebigite-type structure dominates the speciation. For intermediate to high U loadings, one may propose that the speciation is dominated by a change of conformation in which the uranyl carbonate complex mixes bidentate and monodentate structures and may correspond to U incorporated into trigonal calcite.

A double mechanism shall then be considered for U retention onto carbonate minerals consistent with models developed for sorption and coprecipitation into calcite. It is based on the rearrangement of the uranyl equatorial oxygen coordination in a tricarbonate complex as a function of uranyl environmental conditions.¹²⁵⁻¹²⁷

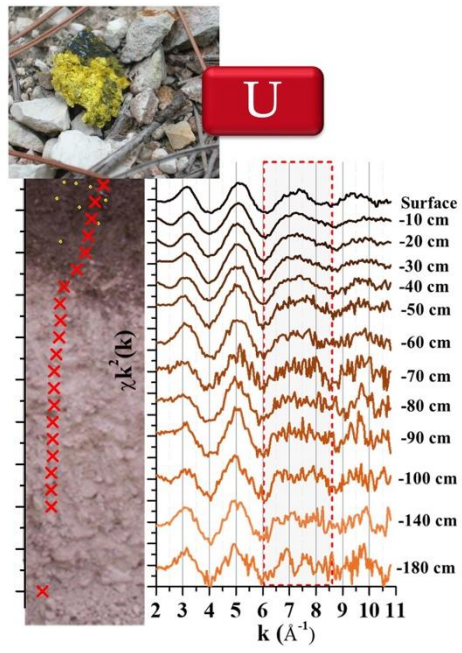
Supporting Information

Supporting Information file is provided with 3 sections: 1. Natural soil characteristics; 2. Modelling of sorption isotherms; 3. EXAFS and TRIFS spectra of the uranium model compounds.

Acknowledgements

This worked was financed by Commissariat à l'Energie Atomique et aux Energies Alternatives, Synchrotron SOLEIL and Université Côte d'Azur with the contribution of Academy *Space Environment, risk and resilience* of Université Côte d'Azur (through the UCAJEDI Investments in the Future project managed by the National Research Agency (ANR) with the reference number ANR-15-IDEX-01).

TOC Art



Figures

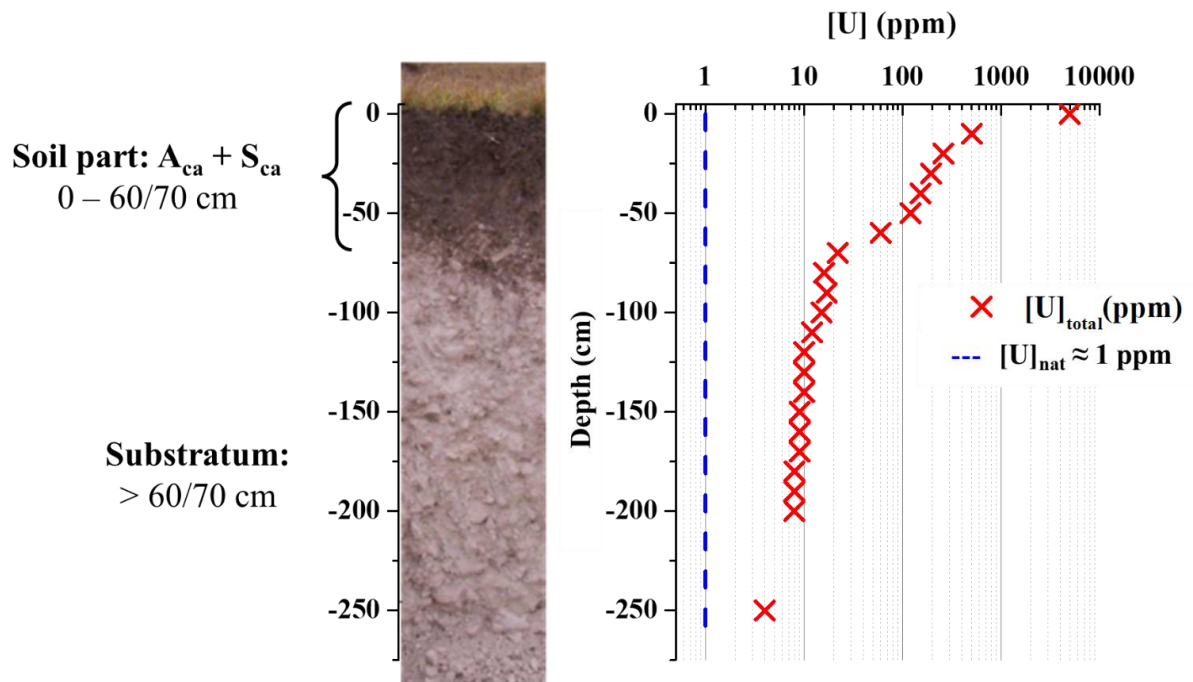


Figure 1: Evolution of mass uranium content in ppm (right graph) in soil and chalk along a vertical profile from the study site. Schematic subsoil structure is given on the left, from the topsoil layer to the chalk substratum down to 2.7 m deep.

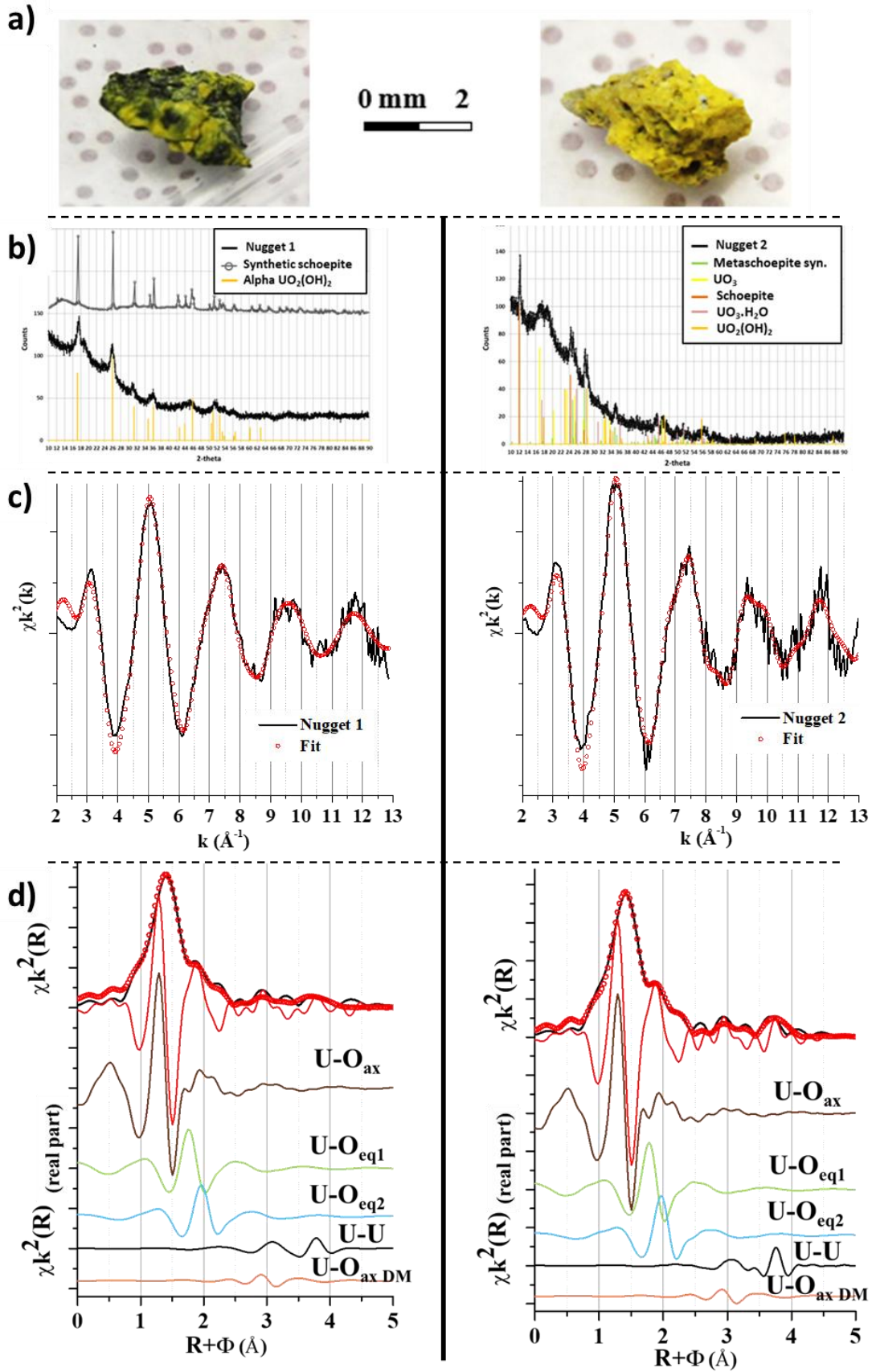


Figure 2abcd: a) Pictures of altered uranium nuggets from the study site: left, dark yellow altered nugget (nugget #1), right, yellowish altered nugget (nugget #2). b) XRD diffractograms of nuggets 1 and 2 (left and right respectively) in comparison with some references of interest. c) EXAFS spectra

(black line) and fit (red circles) of nuggets 1 and 2 (left and right). d) Fourier transform of the EXAFS spectra and real part of the different contributions from the fit of EXAFS spectra of nuggets 1 and 2 (left and right).

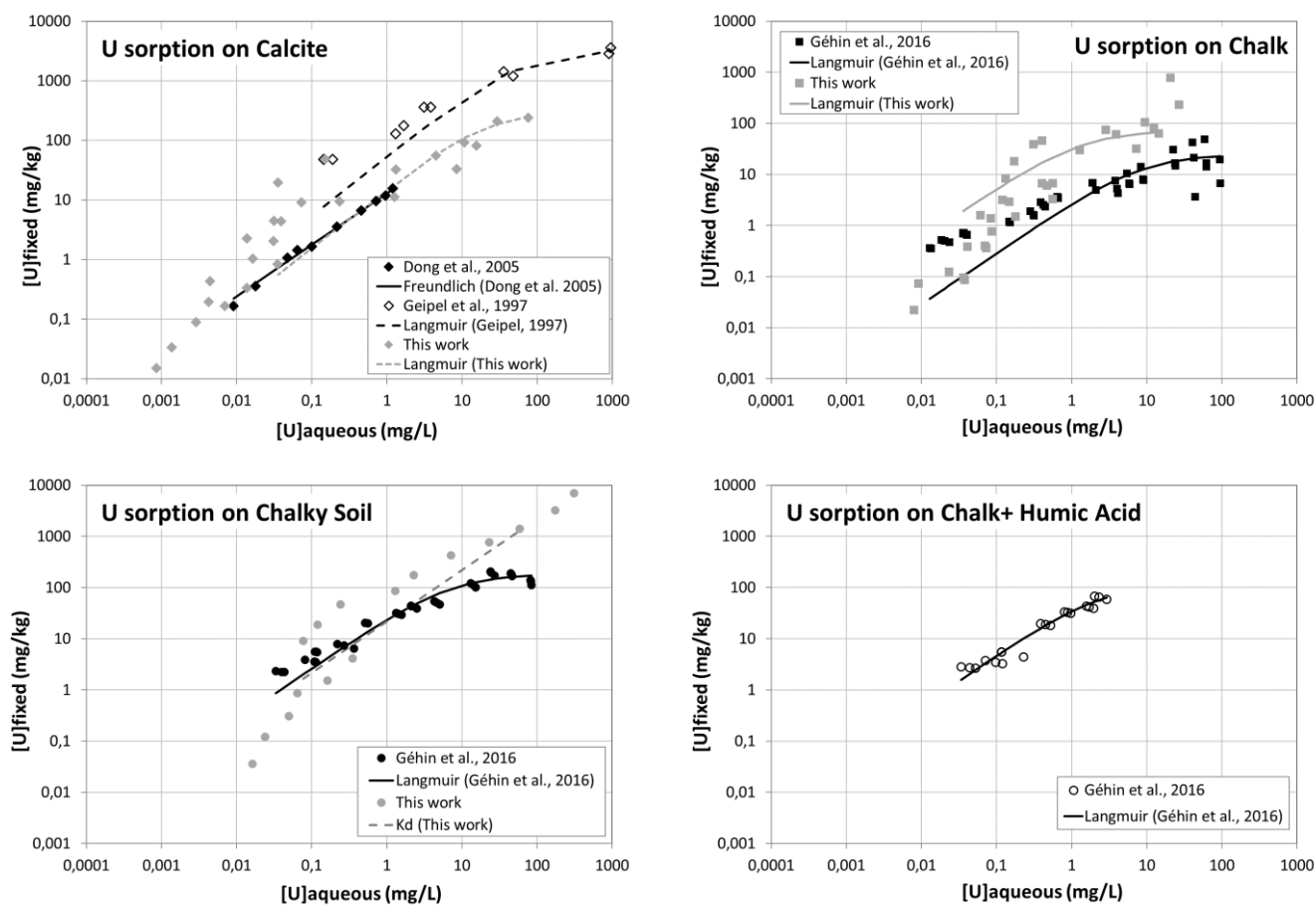


Figure 3. Experimental adsorption isotherms of uranyl onto solid carbonates substrates (pure calcite, chalk and chalky soil) with corresponding modelling using K_d , Freundlich or Langmuir adjustments. Experimental isotherms data are collected from this work, from older experiments on the same sorbents (Géhin et al., 2016⁷⁹), and from bibliography on pure Calcite (Dong et al., 2005⁸⁷; Geipel et al., 1997⁸⁸).

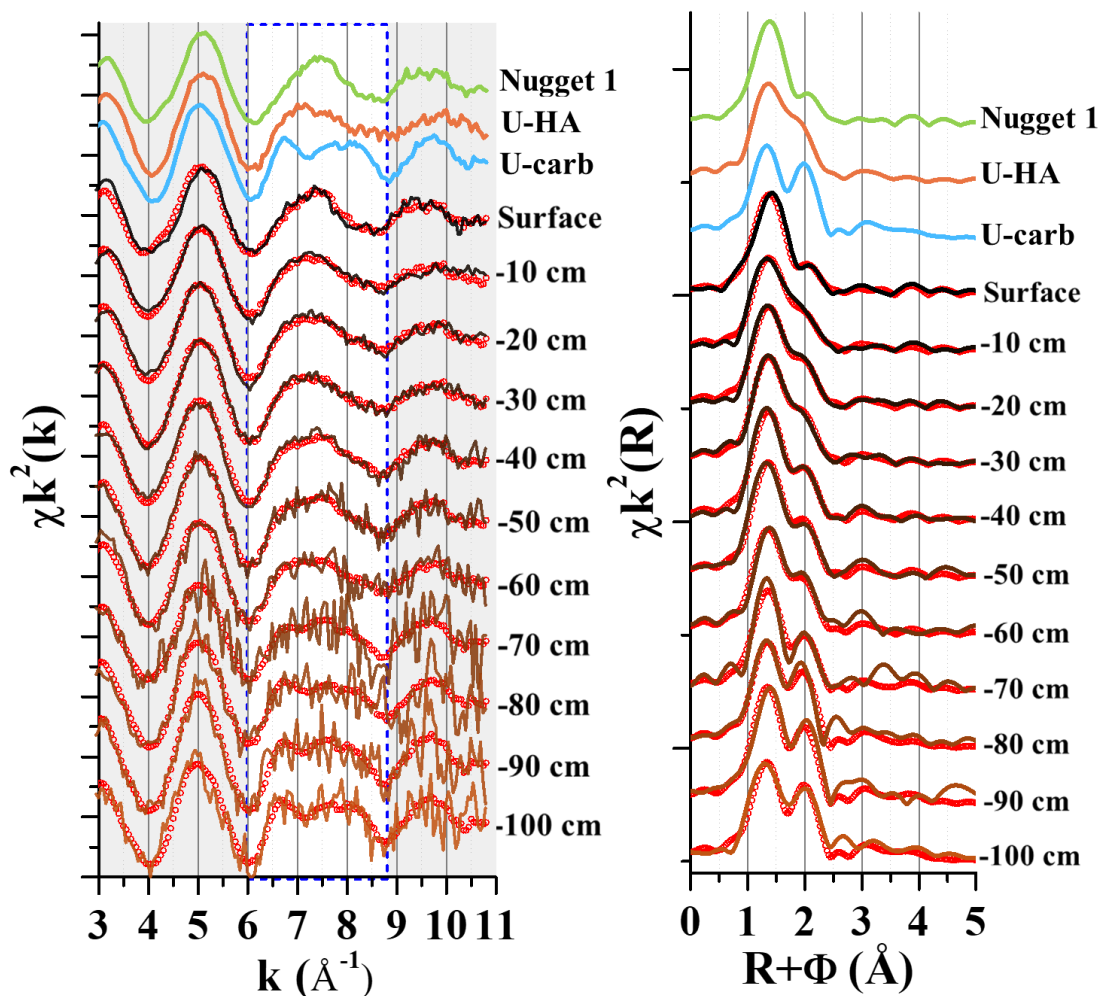


Figure 4: EXAFS spectra (left) and Fourier transform (right) of reference material for uranyl speciation (green: U-nugget #1 in green, brown: U sorbed on HA, and blue: uranyl-tricarbonate complex), together with the series of discrete samples from the vertical soil profile (black to brown faded colored spectra) from surface to 100 cm deep. In red are presented the Linear Combination Fittings of experimental spectra (left), and the real part of the different contributions (right). The integration window of the Fourier transform is of Hanning type and is conducted between $k = 3$ to 11\AA^{-1} .

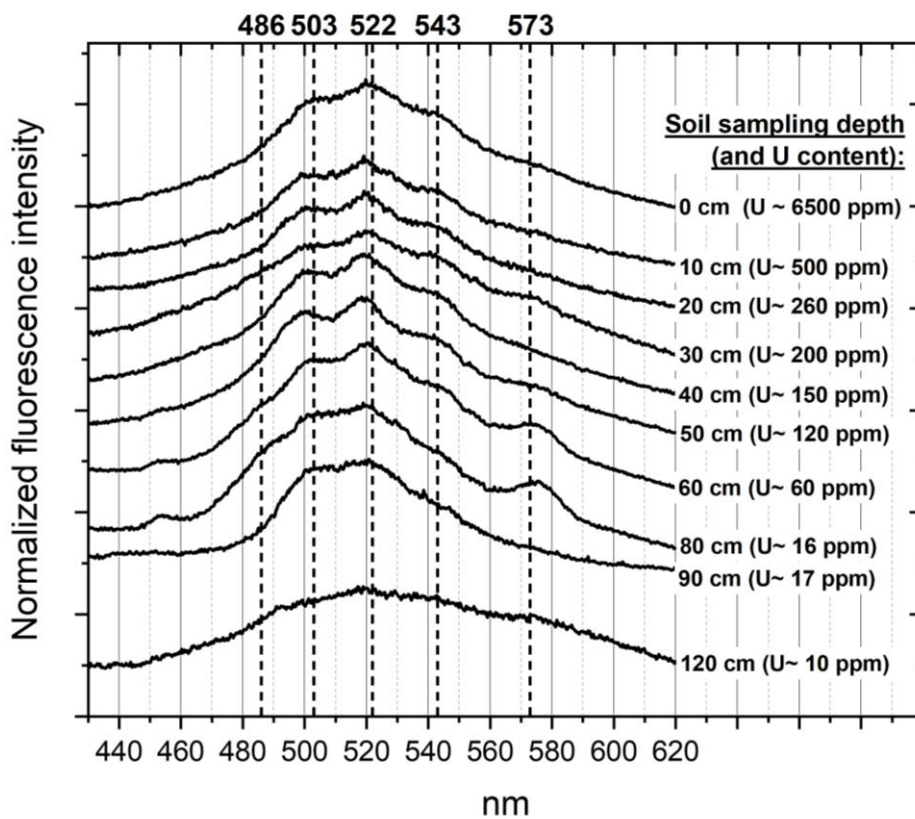


Figure 5: Compared normalized fluorescence spectra of uranium in a chalky soil vertical profile from the study site, with decreasing U content with depth. Spectra were acquired with a delay of 5 μ s with a gate width of 20 μ s, by stacking 500 repetitions. The main fluorescence emission lines of uranyl tricarbonate specie 1 (Liebigite-type structure) are reported in dashed lines.

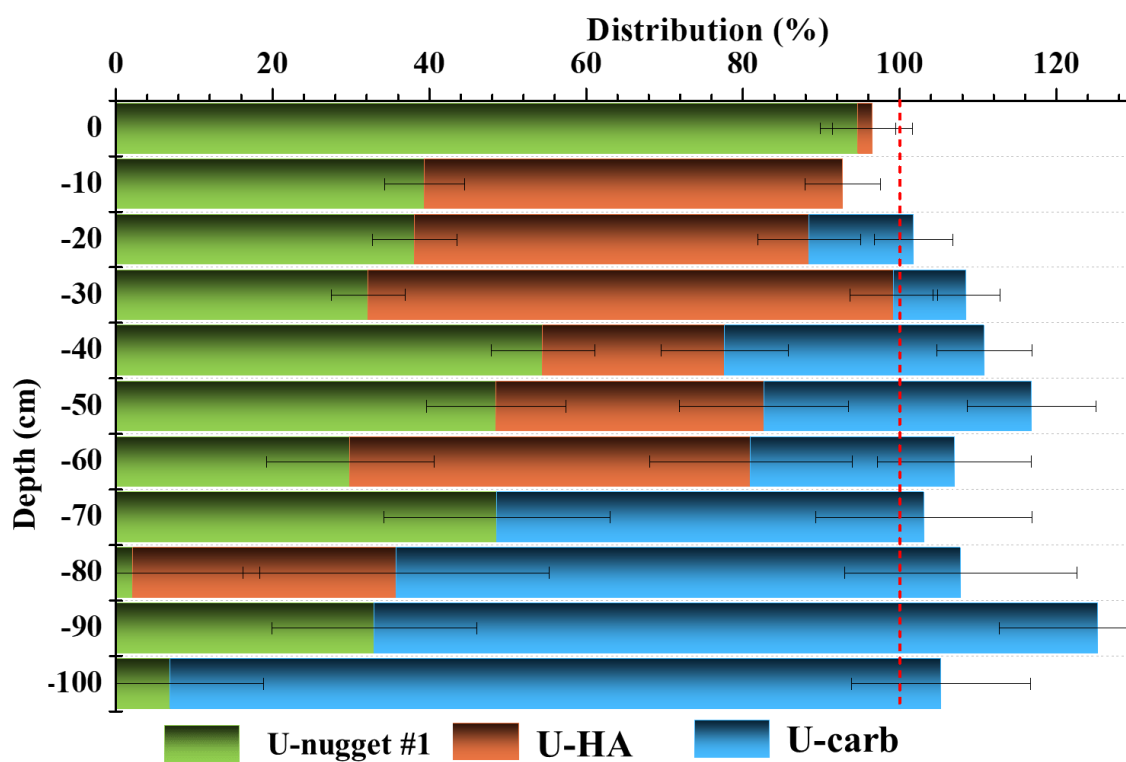


Figure 6: Compared evolutions of soil uranium content (right) and normalized uranium speciation along the soil vertical profile (left), as estimated from LCF on EXAFS analysis using a 3-components model.

Supporting Information file

Uranium speciation in a chalky soil

Simon Bayle^{1,2,3} (ORCID 0000-0003-3851-5459), Maria Rosa Beccia¹ (ORCID 0000-0001-5397-9759), Christophe Moulin^{3,4}, Pier Lorenzo Solari^{2*}, Christophe Den Auwer^{1*} (ORCID 0000-0003-2880-0280), Pierre Crançon^{3*} (ORCID 0000-0002-9207-2663)

1 Université Côte d'Azur, CNRS, ICN, 06108 Nice, France

2 Synchrotron SOLEIL, L'Orme des Merisiers, Départementale 128, F-91190, Saint-Aubin, France

3 CEA, DAM, DIF, F-91297 Arpajon, France.

4 Secrétariat Général à la Défense et Sécurité Nationale, F-75007, Paris, France

Pier Lorenzo Solari, pier-lorenzo.solari@synchrotron-soleil.fr

Christophe Den Auwer, christophe.denauwer@univ-cotedazur.fr

Pierre Crançon, pierre.crancon@cea.fr

SI file content :

- 26 pages

- 3 sections with 13 Figures and 7 Tables

1. Natural soil characteristics

Table S1 : Summary of the mineralogical and organic composition (given in mass. %) and bulk uranium content (in ppm) of the soil and chalk samples from the study site (modified from Gillon et al., 2010).¹

Sample	Mineralogical composition (mass.%)							(ppm)	
	Calcite + Dolomite	Feldspars + Micas	Kaolinite	Silica	Gibbsite	Fe-oxides	Organic Matter	U	
Topsoil - colluvium*	59%	11%	17%	6%	0%	3%	4%	1-2	
Soil profile samples (contaminated area)	0	87%	3%	2%	0%	2%	1%	5%	6358
	-10	86%	3%	4%	0%	2%	1%	4%	502
	-20	87%	3%	3%	0%	2%	1%	3%	260
	-30	88%	3%	4%	0%	2%	1%	3%	195
	-40	89%	3%	4%	0%	2%	1%	2%	152
	-50	91%	2%	3%	0%	2%	1%	1%	120
	-60	93%	2%	1%	0%	2%	1%	0.2%	60
	-70	95%	2%	1%	0%	2%	1%	0.3%	22
	-80	95%	2%	1%	0%	2%	0%	0.3%	16
	-90	96%	1%	0%	0%	2%	0%	0.3%	17
	-100	94%	2%	0%	0%	2%	1%	0.3%	15
	-200	96%	1%	0%	0%	2%	0%	0.1%	8
	-250	97%	1%	0%	0%	2%	0%	0.1%	4
Chalk substrate*	96%	2%	0%	0%	1%	0%	0.2%	1	

*: references values in the geochemical background outside contaminated area

Table S2. Specific surfaces of solid phases samples used as adsorbent in sorption experiments.

Sample type	Specific surface (BET) (m ² .g ⁻¹)	Reference
Purified Calcite	2.2	Vdovic 2001 ²
Chalk	3.2 ± 0.1	This work
Chalky soil	5.4 ± 0.3	This work

Table S3. Concentration of the different elements composing the electrolyte

	Concentration (mmol.L⁻¹)
HCO₃⁻	3.8
Ca²⁺	2.2
Mg²⁺	0.03
Sr²⁺	0.004
Na⁺	0.168
K⁺	0.024
Cl⁻	0.487
NO₃⁻	0.218
SO₄²⁻	0.068
F⁻	0.019
SiO₂(aq)	0.067

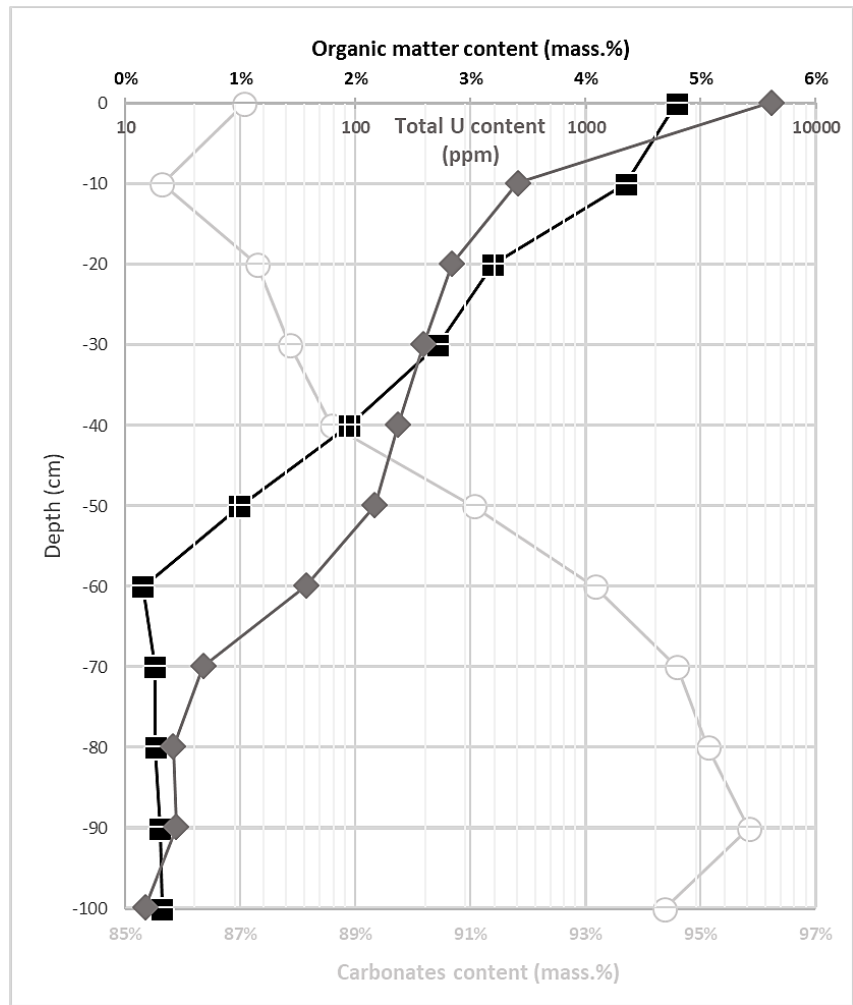


Figure S1: Mass distribution of total carbonate content (grey and white circles, in mass.%), total organic matter content (black squares, in mass.%), and uranium (grey diamonds, in ppm) as a function of depth in soil in the study site.

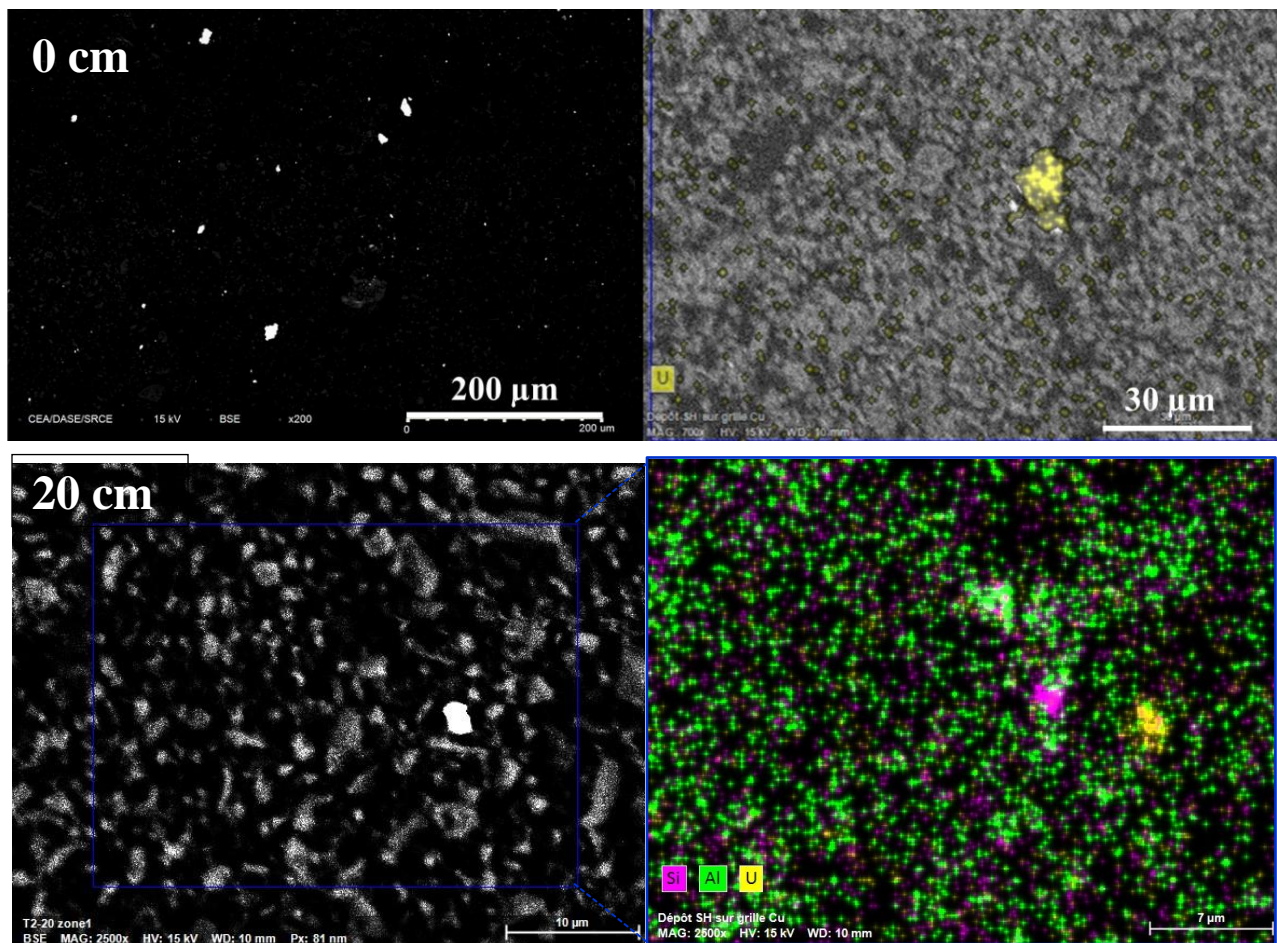


Figure S2. Electron microscope imaging showing the presence of uranium microparticles in the surface soil sample (0 cm, top images) and at 20 cm deep (bottom images) of a vertical profile realized in the chalky soil from the study site. Backscattered electron imaging (on left) shows the presence of multiple U particles lower in size to 50 μm , as well as fluorescence mapping using EDX at the U L- α edge (on right).

2. Modelling of sorption isotherms

K_d Isotherm

K_d isotherm describes the simplest adsorption process in which the amount of surface adsorbate is proportional to the concentration of adsorbate in the aqueous phase. This linear isotherm model describes an appropriate fit to the adsorption of adsorbate at relatively low concentrations, assuming an homogeneous surface and no maximum sorption capacity for the sorbent (Ayawei 2017).³ The default stoichiometry (fixed adsorbate on the surface $\equiv X$:adsorbate in solution at equilibrium) in the sorption reaction is assumed to be equal to (1:1), as shown hereafter for the example of uranyl ion :



The sorption concentration on the substrate at equilibrium, q_{eq} (mg.kg⁻¹), and the distribution coefficient K_d (L.kg⁻¹) were calculated for uranium using the following equations:

$$q_{eq} = (c_0 - c_{eq}) \times \frac{V}{m} \quad (7)$$

$$K_d = \frac{c_0 - c_{eq}}{c_{eq}} \times \frac{V}{m} = \frac{q_{eq}}{c_{eq}} \quad (8)$$

Where q_{eq} (mg.kg⁻¹) is the amount of the uranium sorbed onto the calcite substrate at equilibrium respectively, c_0 (mg.L⁻¹) is the initial concentration of uranium in the aqueous solution, c_{eq} (mg.L⁻¹) is the equilibrium concentration of uranium in the solution, V (L) is the volume of the solution and m (kg) is the weight of the substrate.

Freundlich Isotherm

The Freundlich equation is an empirical expression for non-linear adsorption equilibrium, widely used in environmental soil chemistry to describe the isothermal variation of gas or solute adsorption (Sparks 2003). Freundlich isotherm is applicable to adsorption processes that occur on heterogeneous surfaces, and defines the surface heterogeneity and the exponential distribution of active sites and their energies. It can be expressed as:

$$q_{eq} = K_F \times c_{eq}^n \quad (9)$$

Where q_{eq} and c_{eq} were defined earlier, K_F is the distribution coefficient, and n is a correction factor.

The following equation represents the linear form of the Freundlich a Freundlich isotherm (Boparai, Joseph et al. 2011):

$$\log q_{eq} = \log K_F + n \log c_{eq} \quad (10)$$

The single K_F term in the Freundlich equation implies that the energy of adsorption on a surface is independent of surface coverage. Thus, one of the major disadvantages of the Freundlich equation is that it does not predict an adsorption maximum, failing at high adsorbate concentration in the aqueous phase. The value of n can be between 0 and 1, therefore the equation holds well only over a limited range of dissolved adsorbate concentration:

- when $n = 0$, the adsorption is independent of adsorbate concentration in solution,
- when $n = 1$, adsorption is directly proportional to adsorbate concentration in solution (equivalent to Kd isotherm).

Langmuir Isotherm

Langmuir isotherm was primarily designed to describe gas-solid phase adsorption, and is also used to qualify and quantify the adsorptive capacity of various adsorbents (Sparks 2003).⁴ The Langmuir isotherm accounts for the surface coverage by balancing the relative rates of adsorption and desorption (dynamic equilibrium), and describes a progressively increasing surface occupancy as a function of solute concentration, up until the entire surface area is coated with a monolayer of molecules and no further adsorption can occur (Azizian 2021).⁵

The Langmuir equation can be written in the following linear forms:

$$\frac{c_{eq}}{q_{eq}} = \frac{1}{q_m K_L} + \frac{c_{eq}}{q_m} \quad \text{or} \quad q_{eq} = \frac{q_m K_L c_{eq}}{1 + c_{eq} K_L} \quad (11), (12)$$

Where q_{eq} and c_{eq} were defined earlier, K_L is the distribution coefficient, and q_m is Langmuir constant related to adsorption capacity ($\text{mg}\cdot\text{kg}^{-1}$) of the sorbent, which implies that larger specific surface area and/or pore volume will result in higher adsorption capacity.

One of the most important assumptions of Langmuir isotherm is one-site occupancy adsorption. Adsorption is proportional to the fraction of the surface of the adsorbent that is open while desorption is proportional to the fraction of the adsorbent surface that is covered (Boparai 2011).⁶

Table S4. Experimental conditions and statistical parameter estimation for uranyl adsorption isotherms on carbonates solid phases from sorption experiments.

Phase type	Source	Experimental data					Isotherm fitting parameters					
		M/V (g.L ⁻¹)	S _{bulk} (m ² .g ⁻¹)	pH	T (°C)	[sites] _{calcite} (μmol/m ²)	Type of model	R ²	RMSE	K(d,F,L) (L.kg ⁻¹)	n	[sites] _{calcite} Q _m (μmol/m ²)
Purified Calcite	Dong 2005 ⁷	100	n.m.	8,4	25	n.m.	Freundlich	0,998	0,24	13,0	0,86	
	Geipel 1997 ⁸	5	6,8	8,6	25	1,2	Langmuir	0,972	211	0,016		2,1
	Elzinga 2004 ⁹	1	10	8,3	25	9	Freundlich	0,964	216	232,5	0,52	
	Niu 2019 ¹⁰	10	n.m.	6,5	25	n.m.	Langmuir	0,970	56	0,068		0,4
	Niu 2019 ¹⁰	10	n.m.	8,5	25	n.m.	Freundlich	0,985	120	75,0	0,6	
	This work	100	2,2	7,0	25	n.m.	Freundlich	0,904	6,2	14,5	0,59	
	This work	100	2,2	9,1	25	n.m.	Langmuir	0,955	22	0,050		0,60
Chalk	Géhin 2016 ¹¹	100	3,2	7,3	12	n.m.	Langmuir	0,556	7,2	0,12		0,03
	Géhin 2016 ¹¹	100	3,2	7,3	12	n.m.	Freundlich	0,515	7,5	5,1	0,35	
	Géhin 2016 ¹¹	100	3,2	7,3	12	n.m.	Kd	0,344	9,6	0,33		
	This work	200	3,2	7,4	25	n.m.	Langmuir	0,999	0,05	1,2		0,01
	This work	200	3,2	7,4	25	n.m.	Freundlich	0,994	0,09	5,4	0,79	
	This work	200	3,2	7,4	25	n.m.	Kd	0,978	0,19	6,3		
	This work	100	3,2	7,4	25	n.m.	Freundlich	0,969	14	26,5	0,66	
	This work	100	3,2	7,4	25	n.m.	Kd	0,970	21,6	9,3		
Chalky soil	Géhin 2016 ¹¹	100	5,4	7,3	12	n.m.	Langmuir	0,892	22,3	0,14		0,24
	Géhin 2016 ¹¹	100	5,4	7,3	12	n.m.	Freundlich	0,799	31,0	39,0	0,35	
	Géhin 2016 ¹¹	100	5,4	7,3	12	n.m.	Kd	0,509	56,5	20		
	This work	200	5,4	7,3	25	n.m.	Langmuir	0,988	1,86	0,02		0,8
	This work	200	5,4	7,3	25	n.m.	Freundlich	0,990	1,86	28,8	1,2	
	This work	200	5,4	7,3	25	n.m.	Kd	0,988	1,86	23,1		
	This work	100	5,4	7,3	25	n.m.	Freundlich	0,959	174	18,8	1,02	
	This work	100	5,4	7,3	25	n.m.	Kd	0,962	157	21,7		
Chalk + Humic Acid	Géhin 2016 ¹¹	100	3,2	7,3	12	n.m.	Langmuir	0,937	5,4	0,41		0,15
	Géhin 2016 ¹¹	100	3,2	7,3	12	n.m.	Freundlich	0,929	5,8	31,8	0,7	
	Géhin 2016 ¹¹	100	3,2	7,3	12	n.m.	Kd	0,901	7,55	26,1		

3. EXAFS and TRLFs spectra of the uranium model compounds

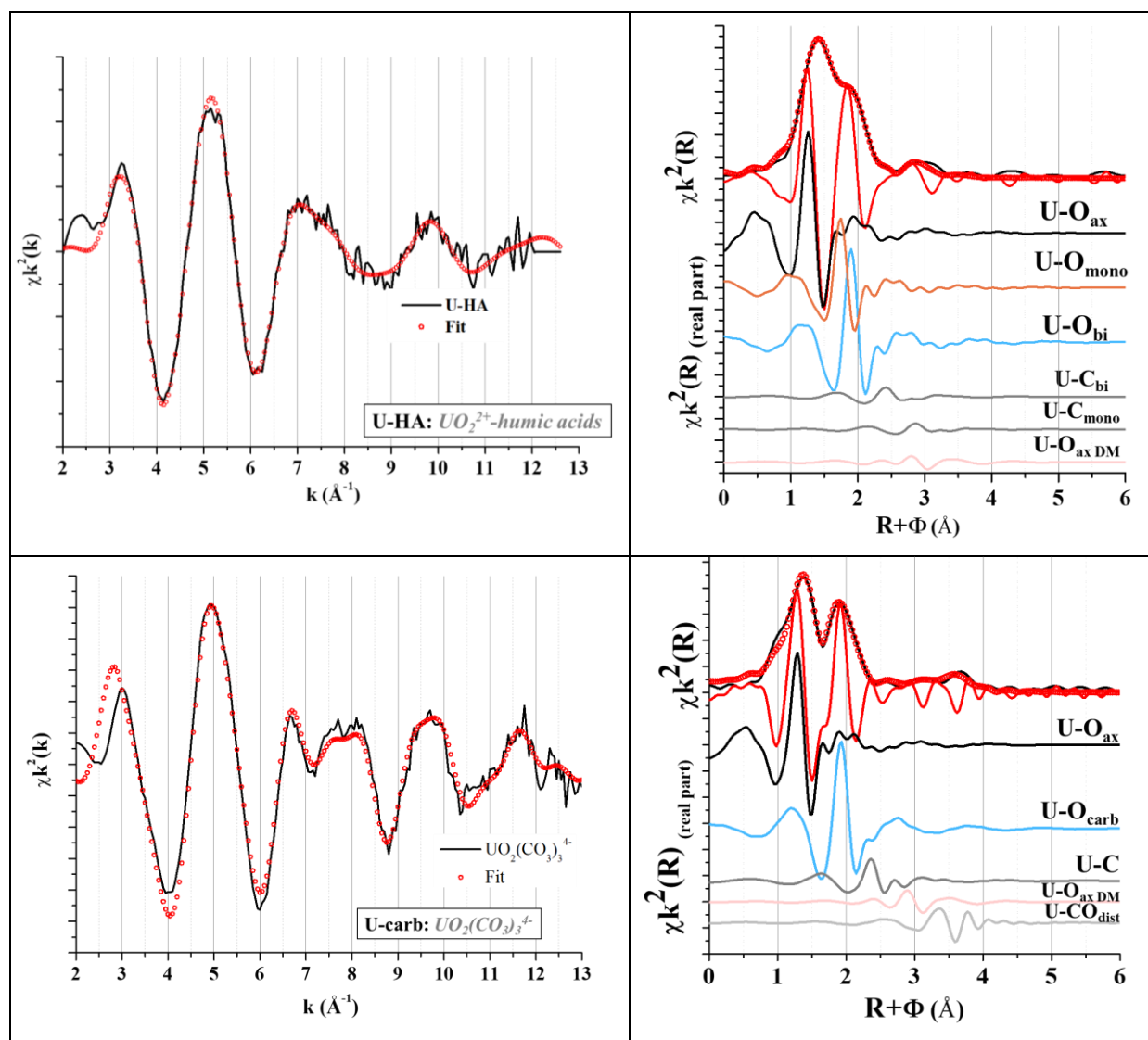


Figure S3: EXAFS spectra (left) and Fourier transform (right) of U sorbed on HA and Uranyl-carb. In red is presented the fit of the data, and in colored the real part of the different contributions. The integration window of the Fourier transform (in blue) is of Hanning type and is between $k = 3$ and $k = 12.5 \text{ \AA}^{-1}$. The spectra, the fit, and the different contributions of the real part are grouped at the bottom. The fit was performed in real space, on a window up to $R = 4$

Table S5: Parameters used for fitting the EXAFS spectra of the reference samples U-nugget #1; U-nugget #2, U sorbed on HA and uranyl tricarbonate complex. For comparison, data from the XRD analysis of metaschoepite and Liebigite are added.

	Contrib.	N	σ^2 (Å ²)	R (Å)	e_0 ; S_0^2 ; χ_{red}^2 ; R_f (%)
Nugget 1	U-Oax	2	0.004	1.82 ± 0.01	
	U-Oeq1	2.4 ± 0.2	0.013	2.31 ± 0.01	
	U-Oeq2	2.4 ± 0.2	0.013	2.50 ± 0.01	4.6; 1.0; 8.6; 0.9
	U-U	3.5 ± 0.3	0.019	3.92 ± 0.02	
	U-Oax_MD	4	0.008	3.64	
Nugget 2	U-Oax	2	0.003	1.82 ± 0.01	
	U-Oeq1	2.4 ± 0.2	0.009	2.33 ± 0.01	
	U-Oeq2	2.4 ± 0.2	0.009	2.51 ± 0.01	5.6; 1.0; 3.1; 1.1
	U-U	2.4 ± 0.3	0.009	3.90 ± 0.02	
	U-Oax_MD	4	0.006	3.64 ± 0.02	
Méta-schoepite (Froideval 2006) ¹²	U-Oax	2	-	1.79 ± 0.01	
	U-Oeq1	1.9 ± 0.4	-	2.32 ± 0.02	
	U-Oeq2	1.8 ± 0.4	-	2.51 ± 0.02	
	U-U	1.9 ± 0.4	-	3.91 ± 0.02	
Shoepite (Walsh 2014) ¹³	U-Oax	1.9 ± 0.2	-	1.77 ± 0.01	
	U-Oeq1	3.5 ± 1.0	-	2.32 ± 0.02	
	U-Oeq2	2.4 ± 0.6	-	2.51 ± 0.02	
Shoepite (Allen 1996) ¹⁴	U-Oax	1.7 ± 0.3	-	1.81 ± 0.01	
	U-Oeq1	2.1 ± 0.5	-	2.26 ± 0.02	
	U-Oeq2	1.9 ± 0.5	-	2.47 ± 0.02	
	U-U1	1.2 ± 0.4	-	3.84 ± 0.02	
	U-U2	1.4 ± 0.4	-	4.53 ± 0.02	
U-HA <i>UO₂²⁺-Humic acids</i>	U-Oax	2*	0.003	1.80 ± 0.01	
	U-Omono	2.5 ± 0.1	0.003	2.29 ± 0.01	
	U-Obi	3.0 ± 0.2	0.003	2.44 ± 0.01	6.2; 1.2; 2.1; 0.3
	U-Cmono	N(Omono)	0.013	3.03 ± 0.02	
	U-Cbi	N(Obi)/2	0.013	3.49 ± 0.02	
U-carb <i>UO₂(CO₃)₃⁴⁻</i>	U-Oax	2*	0.003	1.82 ± 0.01	6.9; 1.0; 7.0; 0.3
	U-Ocarb	6*	0.011	2.45 ± 0.01	

Liebigite (Bernhard 2001) ¹⁵	U-C	3*	0.008	2.93 ± 0.01
	U-COdist	6*	0.02	4.02 ± 0.02
	U-Oax	2		1.80 ± 0.01
	U-Ocarb	6		2.43 ± 0.01
	U-C	3		2.88 ± 0.01
	U-Ca	2		4.02 ± 0.02

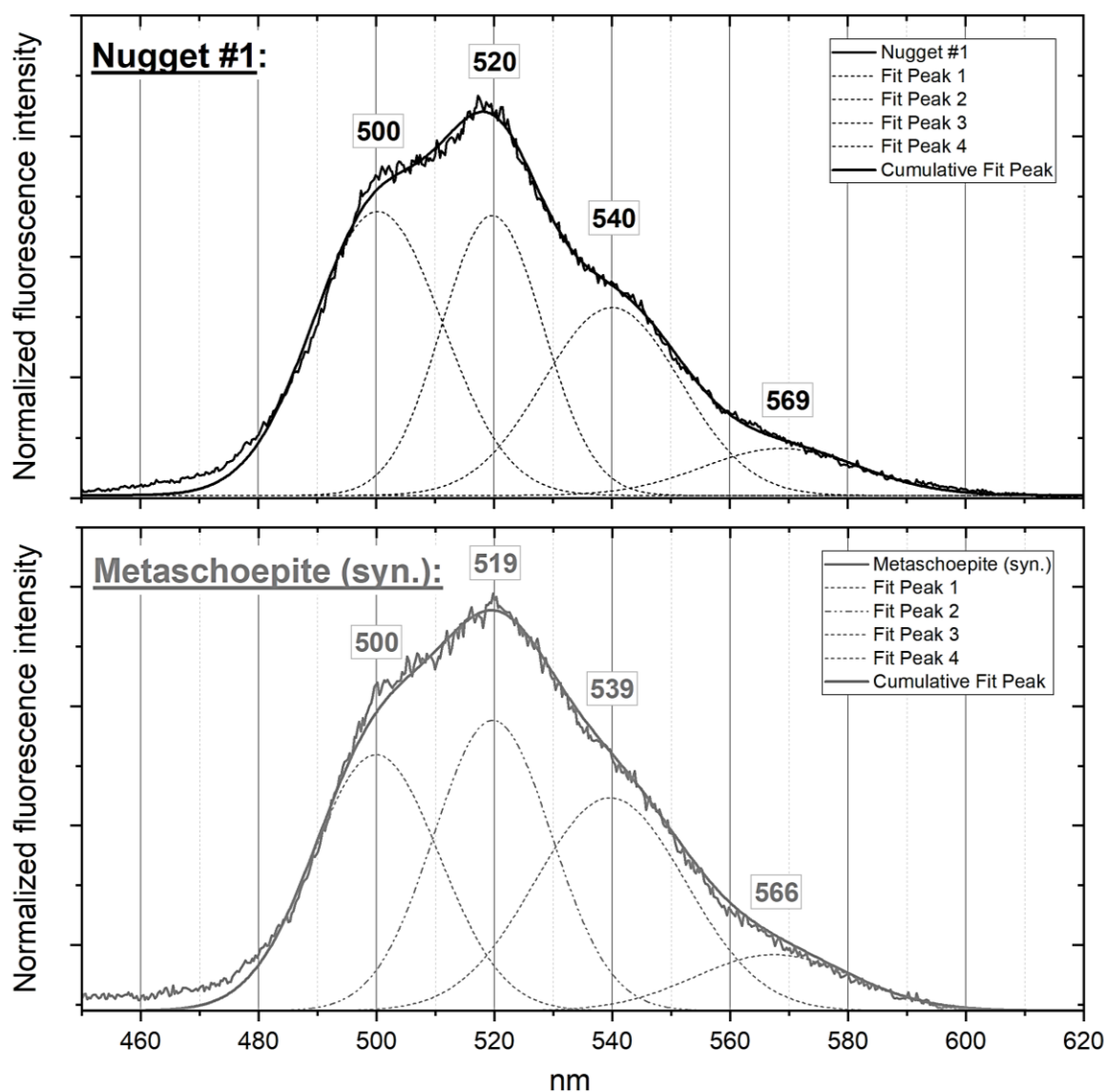


Figure S4: Normalized fluorescence spectra of uranium nugget#1 (top, dark curves) and synthetic metaschoepite (bottom, dark grey curves) at room temperature using an excitation wavelength of 355 nm. Spectrum for metaschoepite is recorded using a delay of 20 μ s and a gate width of 200 μ s. Spectrum for nugget#1 is recorded, using a delay of 100 μ s and a gate width of 200 μ s. The main fluorescence emission lines obtained from spectra deconvolution are reported above the curves (boxes).

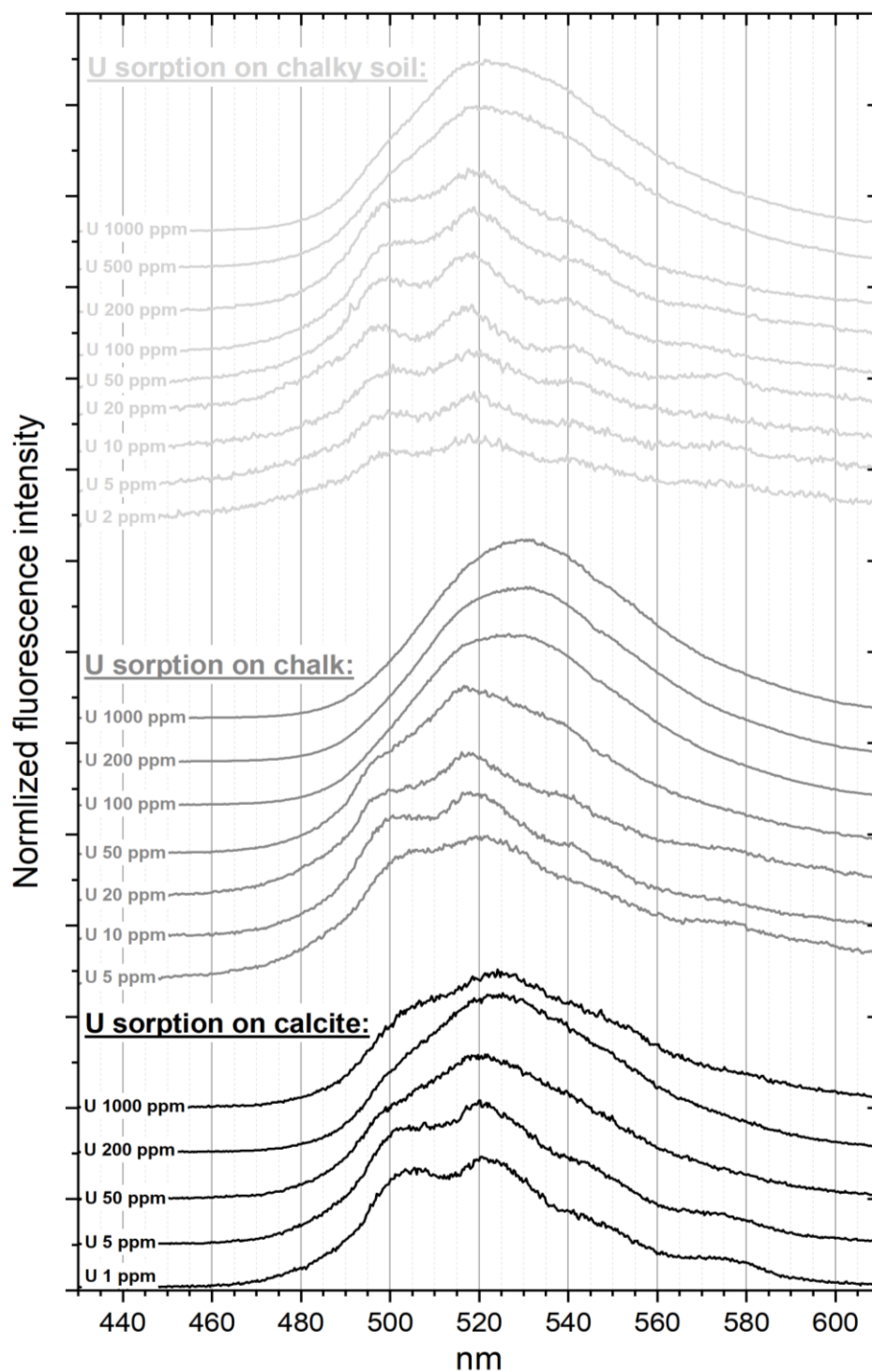


Figure S5: Compared normalized fluorescence spectra of uranium sorbed onto calcite (black curves), onto natural chalk (gray curves), and onto natural chalky soil (light gray curves), for initial dissolved uranium concentration varying from 1 to 1000 ppm. Spectra were acquired with a delay of 100 μ s with a gate width of 50 μ s, by stacking 500 repetitions.

Table S6. Spectral properties and fitting parameters for TRLFS spectra of reference samples (this work, and literature, white cells), and for U(VI) sorbed onto calcite and chalk (gray cells).

Reference samples & data :	Spectral maxima, nm (Width, nm)					fit R ²	Timelife τ , μ s	Source	
Uranyl hydrates									
Metaschoepite (syn.)	500 (21)	519 (20)	539 (26)	566 (28)		0,993	50	This work	
Nugget #1	500 (22)	520 (17)	540 (23)	569 (27)		0,997	131	This work	
<i>Metaschoepite</i>	511	527	552				17	Wang 2008 ¹⁶	
<i>Schoepite</i>	514 (26)	532 (22)	552 (25)	580 (36)			21	Wang 2008 ¹⁶	
Uranyl carbonates									
Liebigite (nat.)	466 (7)	486 (10)	506 (13)	525 (18)	548 (17)	565 (33)	0,980	184	This work
<i>Liebigite (nat.)</i>	463 (7)	481 (10)	502 (13)	524 (12)	548 (17)	574 (14)		349	Wang 2008 ¹⁶
<i>U incorporated in Aragonite</i>		484 (11)	503 (13)	525 (15)	546 (14)	560 (45)			Elzinga 2004 ⁹
<i>U incorporated in Calcite</i>			497 (13)	517 (16)	537 (19)	555 (34)			Elzinga 2004 ⁹
Experimental results :									
U sorbed on Calcite (specie 1 : liebigite-type structure)	489 (24)	505 (19)	524 (15)	543 (19)	570 (27)		0,999	220	This work
U sorbed on Calcite (specie 2)	488 (20)	498 (12)	517 (14)	539 (15)	565 (16)		0,982	n.d.	This work

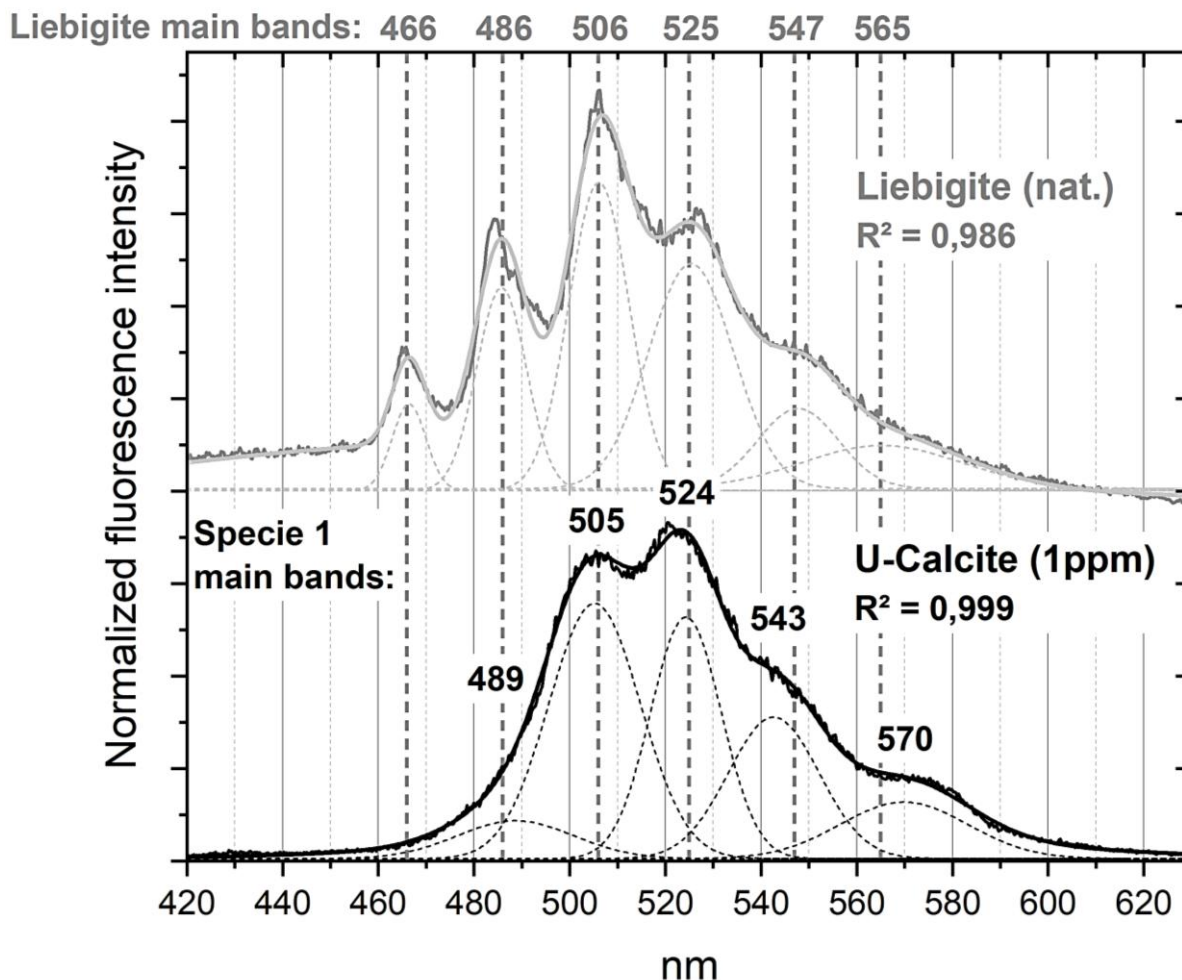


Figure S6. Normalized fluorescence spectra of uranium sorbed onto Calcite for initial dissolved uranium concentration of 1 ppm. The spectrum deconvolution is achieved considering five major vibronic bands resolved as Gaussian peaks. Peaks positions, reported in boxes, are comparable with published spectral data on U(VI)-substituted synthetic calcite and aragonite, in a Liebigite-like structure (Elzinga 2004⁹, Wang 2005¹⁷, Wang 2008¹⁶). The TRLFS spectrum of a natural uranyl calcium triscarbonate mineral (liebigite) has been recorded with 200 μ s delay and exhibits 6 major maxima fairly consistent, with a slight red-shift, with other luminescence data found in literature for liebigite, uranium incorporated in aragonite in a triscarbonate structure, or calcium-uranyl triscarbonate aqueous complex.

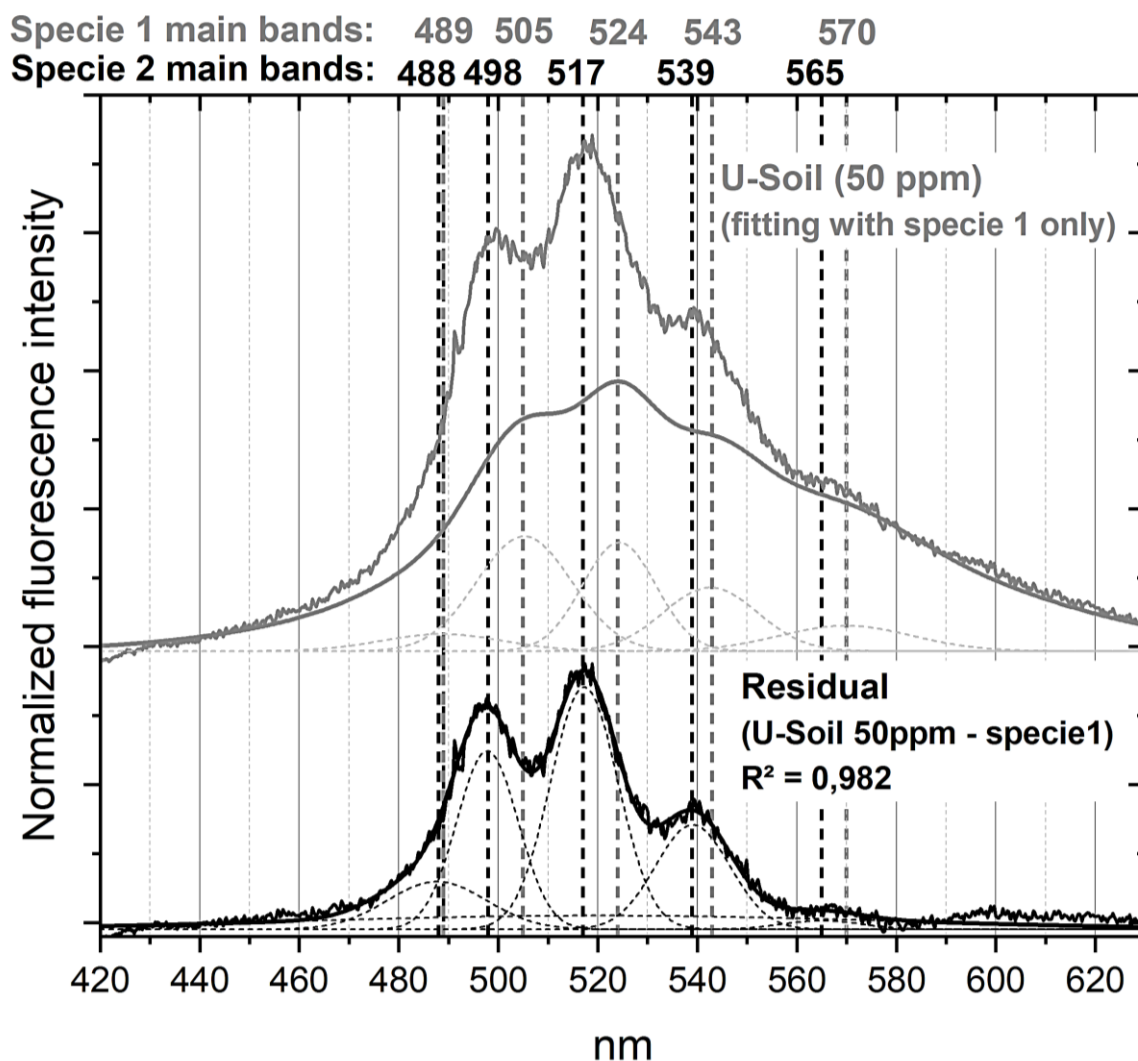


Figure S7: Determination of fluorescence bands of U(VI)-carbonate sorbed second specie in residuals (in gray) after subtraction of liebigite cumulative peaks from raw fluorescence spectrum of U(VI) sorbed onto chalk for initial dissolved uranium concentration of 10 ppm (in black). Residual spectrum deconvolution is achieved considering four major bands resolved as gaussian peaks. Peaks positions, reported in boxes, are comparables with published spectral data for U(VI) incorporated in calcite, as described by Elzinga 2004.⁹

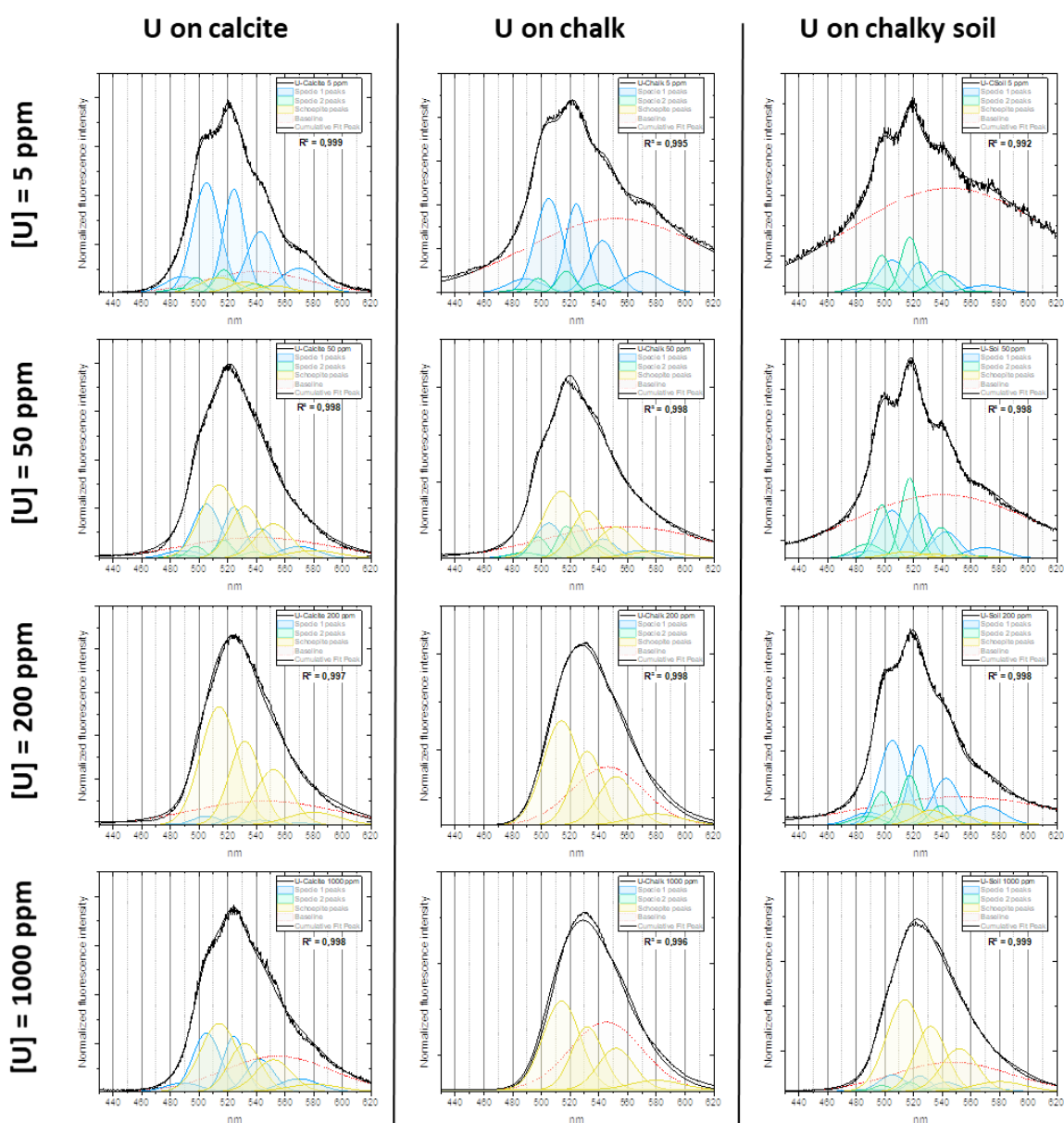


Figure S8: Normalized fluorescence spectra of uranium sorbed onto calcite (left), chalk (center) and chalky soil (right) for initial dissolved uranium concentration varying from 5 to 100 ppm. Detail of spectra deconvolution is reported considering three components: uranyl carbonate with liebigite-type structure (specie 1, in blue), uranyl incorporated in calcite (specie 2, from Elzinga 2004⁹, in green), natural Schoepite (from Wang 2008¹⁶, in yellow). Spectra baseline are fitted considering a Gaussian model, and reported in dashed red line. Deconvolution regression coefficient is given below legends, for indication.

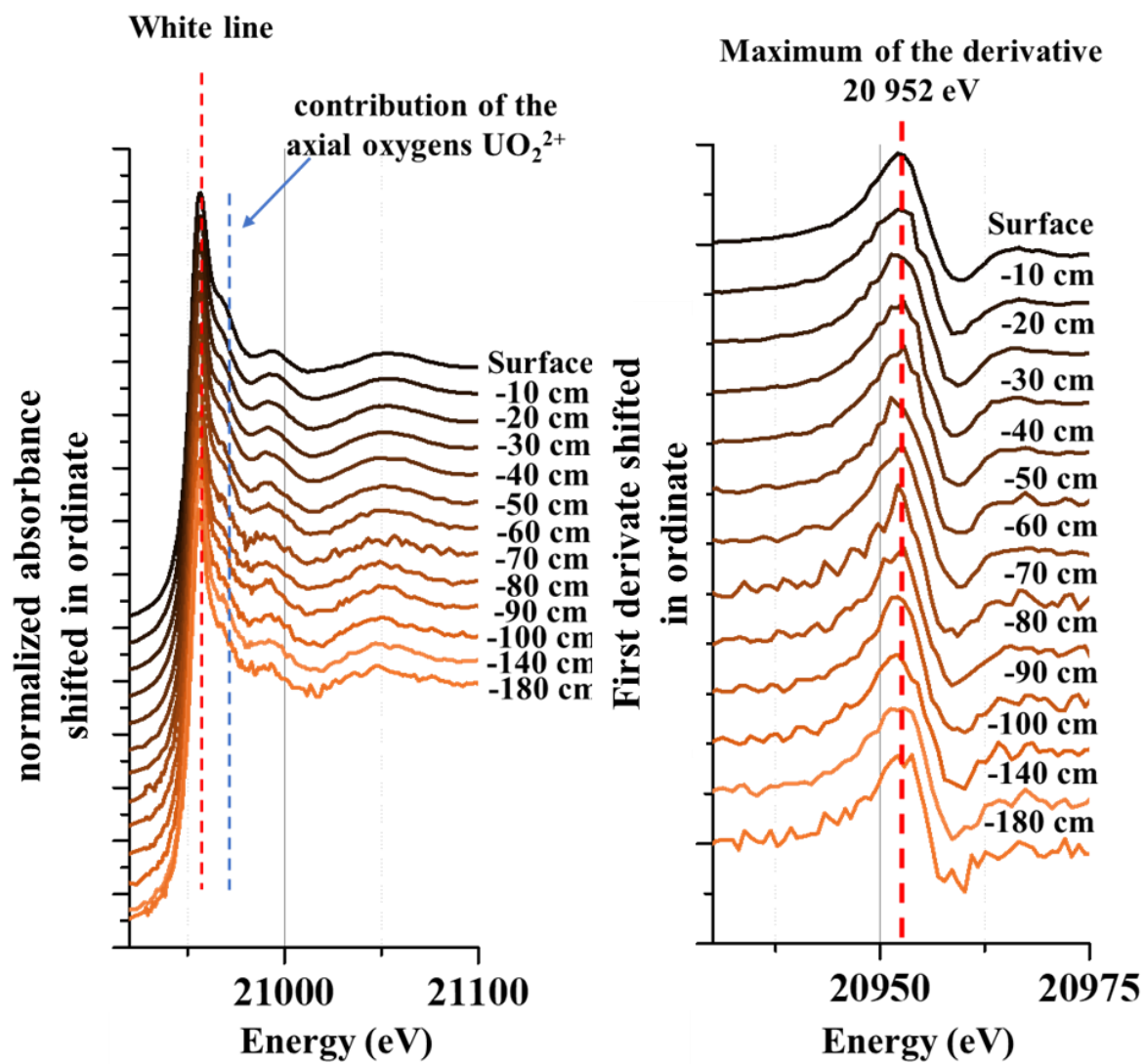


Figure S9: XANES spectra recorded at the U L_{II} edge for soil samples at increasing depth in a vertical profile in the study site (left) and corresponding derivatives (zoom on the edge region, right).

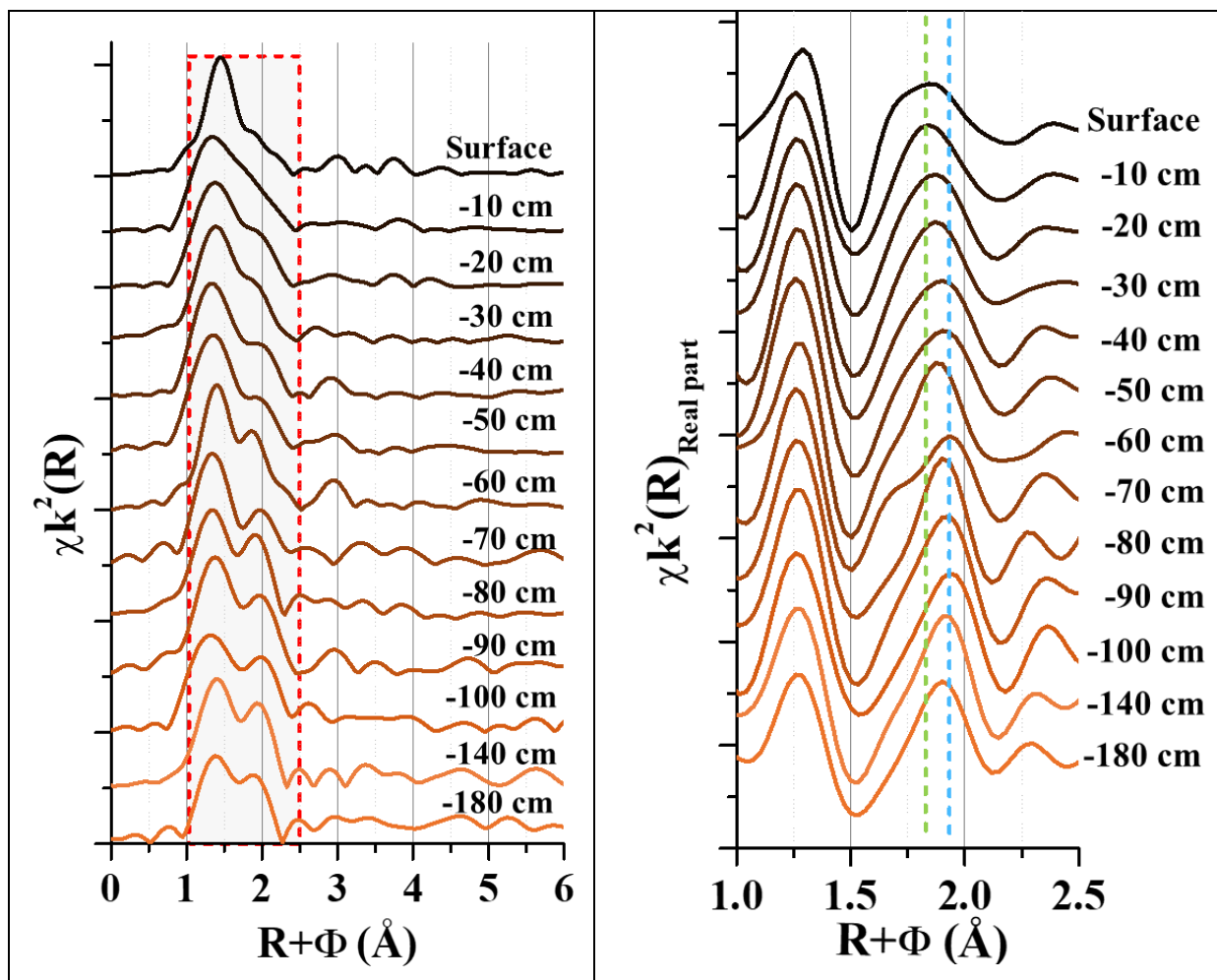


Figure S10: Modulus of the Fourier transform (FT) of the EXAFS spectra recorded at the U L_{II} edge for soil samples at increasing depth in a vertical profile in the study site, (left), and real part of the FT (zoom on the first coordination sphere region, right).

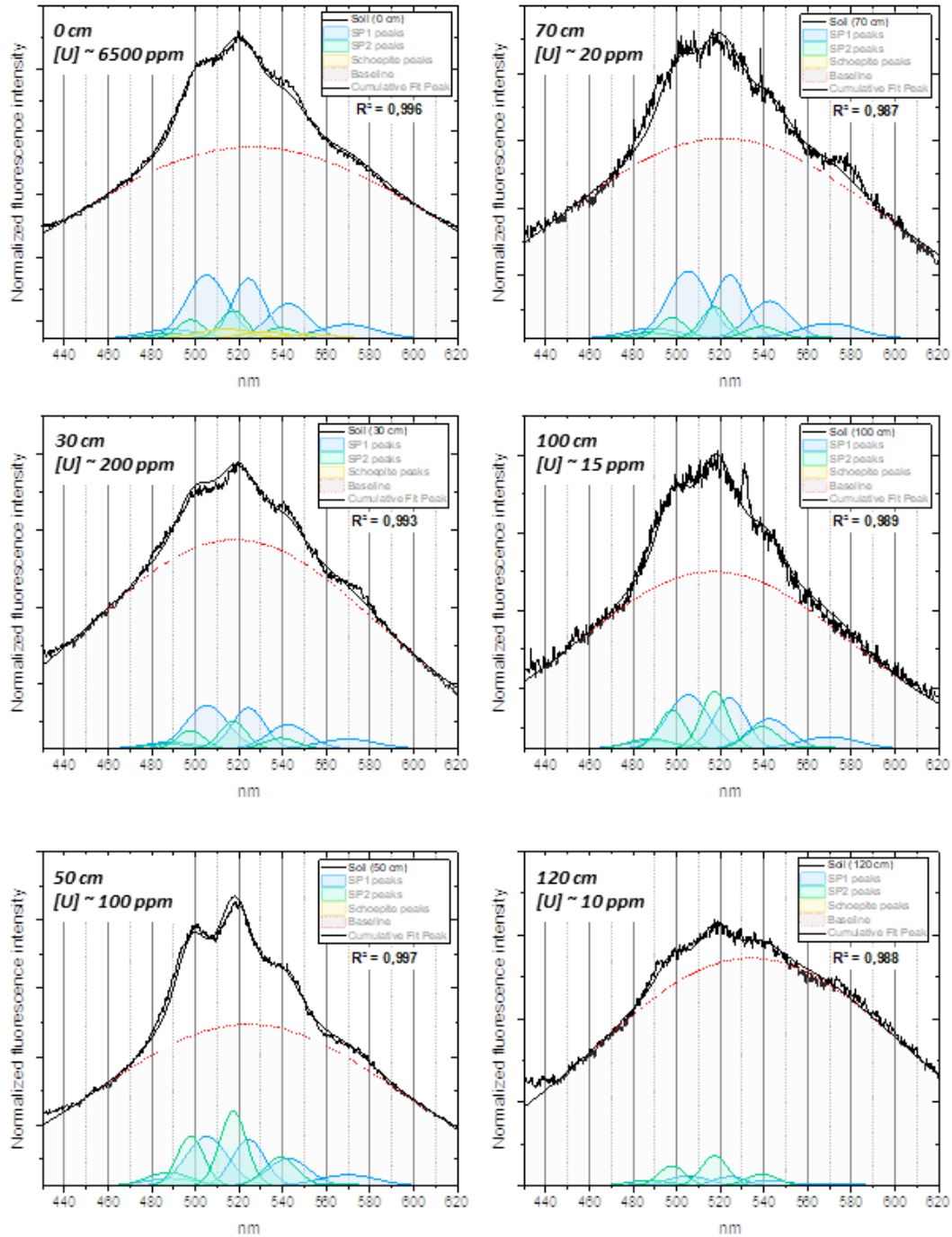


Figure S11: Normalized fluorescence spectra of uranium in a chalky soil profile from the study site, for increasing depth and decreasing U content (soil U content is reminded in the top left corner for each spectrum). Detail of spectra deconvolution is reported considering three components: uranyl carbonate with liebigite-type structure (specie 1, in blue), uranyl incorporated in calcite (specie 2, from Elzinga 2004⁹, in green), natural Schoepite (from Wang 2008¹⁶, in yellow). Spectra baseline are fitted considering a Gaussian model, and reported in dashed red line. Deconvolution regression coefficient is given below legends, for indication

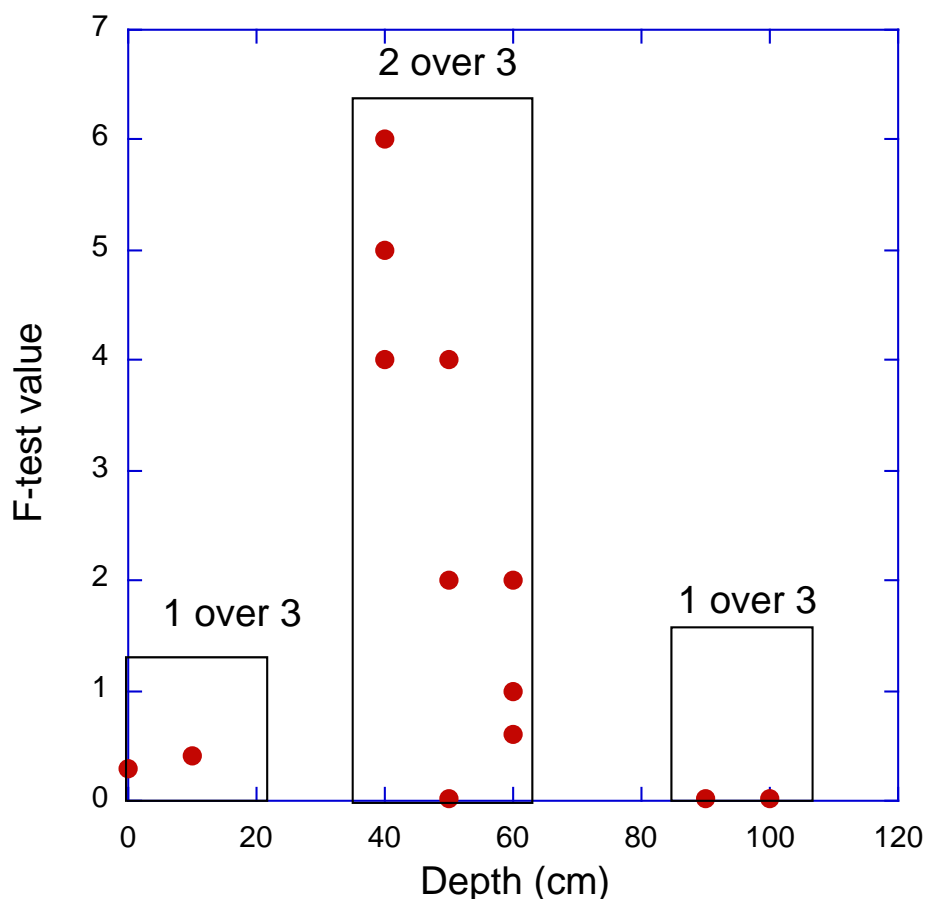


Figure S12: F-test values for 1-component and 2-component fits versus a 3-component fit as a function of depth.

F values are calculated according with “A Variation of the F-Test for Determining Statistical Relevance of Particular Parameters in EXAFS Fits” (Downward 2007¹⁸):

$$F = \frac{(\chi_1^2 - \chi_0^2) / (v_1 - v_0)}{\chi_0^2 / v_0}$$

With:

- χ_1^2 Chi square of tested model
- χ_0^2 Chi square of best model.
- v_1 degrees of freedom of tested model fit.
- v_0 degrees of freedom of best model fit.

The χ^2 values are obtained from ATHENA between $k = 3.5$ and $k = 10.5$ from LCF fitting using 1,2 or 3 components

v the degree of freedom is obtained by subtracting the number of variables from the number of independent points (calculated according with the Stern’s rule (Stern, 1993¹⁹)).

The results show 3 regimes:

(1) the surface and the first few cm can be adjusted properly using a 1-component fit (Nugget) compared to a 3-component fit (F value less than 1).

(2) the soil part of the site (from 20 to 50 cm), cannot be adjusted properly using various combinations of a 2-component fit and requires a 3-component fit (Nugget + U-HA + U-carb) (F values larger than 1).

(3) the substrate part (above 70 cm) of the site can be adjusted with a 1-component fit (U-carb) compared to a 3-component fit (F value less than 1).

The LCF data using 3 components for consistency are in full agreement with this analysis as shown in Figure 6.

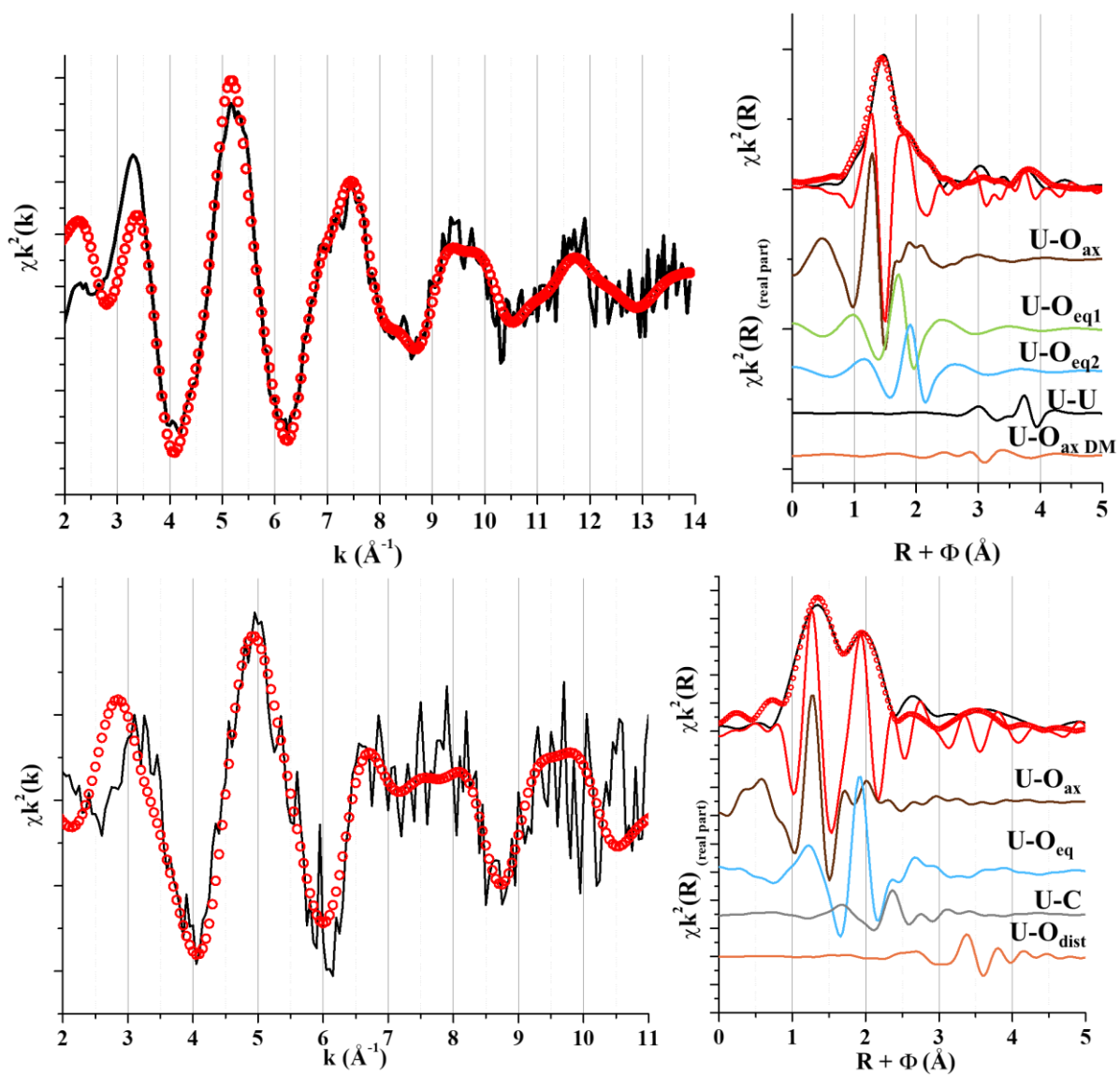


Figure S13: EXAFS spectra at the U L_{II} edge and Fourier transform of the surface sample (0 cm, top) and deepest sample (100 cm, bottom).

Table S7: Best fit parameters of the EXAFS spectra at the U L_{II} edge of the surface sample (0 cm) and deepest sample (100 cm).

	Contribution	N	s^2 (Å ²)	R (Å)	E_0 (eV)	s_0^2	χ_{red}^2	R _{factor} (%)
Surface sample	U-Oax	2	0.004	1.82 ± 0.01				
	U-Oeq1	2.8 ± 0.2	0.010	2.27 ± 0.01				
	U-Oeq2	2.9 ± 0.2	0.010	2.45 ± 0.01	5.2	1	7.9	2.3 %
	U-U	3.0 ± 0.3	0.012	3.91 ± 0.02				
	U-Oax_MD	4	0.008	3.64				
	Contribution	N	s^2 (Å ²)	R (Å)	E_0 (eV)	s_0^2	χ_{red}^2	R _{factor} (%)
100 cm sample	U-Oax	2	0.002	1.81 ± 0.01				
	U-Oeq	6*	0.007	2.44 ± 0.01				
	U-C	3*	0.004	2.9 2± 0.02	6.5	0.9	1.9	3.4 %
	U-Odist	6*	0.004	4.2 ± 0.03				

SI References

- (1) Gillon, M.; Crançon, P.; Aupiais, J. Modelling the Baseline Geochemistry of Groundwater in a Chalk Aquifer Considering Solid Solutions for Carbonate Phases. *Applied Geochemistry* **2010**, *25* (10), 1564–1574.
- (2) Vdović, N. Electrokinetic Behaviour of Calcite—the Relationship with Other Calcite Properties. *Chemical Geology* **2001**, *177* (3–4), 241–248.
- (3) Ayawei, N.; Ebelegi, A. N.; Wankasi, D. Modelling and Interpretation of Adsorption Isotherms. *Journal of Chemistry* **2017**, *2017*, 1–11.
- (4) Sparks, D. L. Sorption Phenomena on Soils. In *Environmental Soil Chemistry*; Academic Press: Burlington, 2003; pp 133–186.
- (5) Azizian, S.; Eris, S. Chapter 6 - Adsorption Isotherms and Kinetic. In *Interface Science and Technology*; Elsevier, 2021; pp 445–509.
- (6) Boparai, H. K.; Joseph, M.; O’Carroll, D. M. Kinetics and Thermodynamics of Cadmium Ion Removal by Adsorption onto Nano Zerovalent Iron Particles. *Journal of Hazardous Materials* **2011**, *186* (1), 458–465.
- (7) Dong, W.; Ball, W. P.; Liu, C.; Wang, Z.; Stone, A. T.; Bai, J.; Zachara, J. M. Influence of Calcite and Dissolved Calcium on Uranium(VI) Sorption to a Hanford Subsurface Sediment. *Environ. Sci. Technol.* **2005**, *39* (20), 7949–7955.
- (8) Geipel, G.; Reich, T.; Brendler, V.; Bernhard, G.; Nitsche, H. Laser and X-Ray Spectroscopic Studies of Uranium-Calcite Interface Phenomena. *Journal of Nuclear Materials* **1997**, *248*, 408–411.
- (9) Elzinga, E. J.; Tait, C. D.; Reeder, R. J.; Rector, K. D.; Donohoe, R. J.; Morris, D. E. Spectroscopic Investigation of U(VI) Sorption at the Calcite-Water Interface. *Geochimica et Cosmochimica Acta* **2004**, *68* (11), 2437–2448.
- (10) Niu, Z.; Wei, X.; Qiang, S.; Wu, H.; Pan, D.; Wu, W.; Fan, Q. Spectroscopic Studies on U(VI) Incorporation into CaCO₃: Effects of Aging Time and U(VI) Concentration. *Chemosphere* **2019**, *220*, 1100–1107.
- (11) Géhin, A.; Markelov, I.; Crançon, P.; Charlet, L. Thermodynamic and Kinetic Properties of U(VI) Sorption on Chalk Substrates, 2016.
- (12) Froideval, A.; Del Nero, M.; Gaillard, C.; Barillon, R.; Rossini, I.; Hazemann, J. L. Uranyl Sorption Species at Low Coverage on Al-Hydroxide: TRLS and XAFS Studies. *Geochimica et Cosmochimica Acta* **2006**, *70* (21), 5270–5284.

- (13) Walshe, A.; Průžmann, T.; Vitova, T.; Baker, R. J. An EXAFS and HR-XANES Study of the Uranyl Peroxides $[\text{UO}_2(\eta^2\text{-O}_2)(\text{H}_2\text{O})_2]\cdot n\text{H}_2\text{O}$ ($n = 0, 2$) and Uranyl (Oxy)Hydroxide $[(\text{UO}_2)_4\text{O}(\text{OH})_6]\cdot 6\text{H}_2\text{O}$. *Dalton Trans.* **2014**, 43 (11), 4400–4407.
- (14) Allen, P. G.; Shuh, D. K.; Bucher, J. J.; Edelstein, N. M.; Palmer, C. E. A.; Silva, R. J.; Nguyen, S. N.; Marquez, L. N.; Hudson, E. A. Determinations of Uranium Structures by EXAFS: Schoepite and Other U(VI) Oxide Precipitates. *Radiochimica Acta* **1996**, 75 (1).
- (15) Bernhard, G.; Geipel, G.; Reich, T.; Brendler, V.; Amayri, S.; Nitsche, H. Uranyl(VI) Carbonate Complex Formation: Validation of the $\text{Ca}_2\text{UO}_2(\text{CO}_3)_3(\text{Aq.})$ Species. *Radiochimica Acta* **2001**, 89 (8).
- (16) Wang, Z.; Zachara, J. M.; Liu, C.; Gassman, P. L.; Felmy, A. R.; Clark, S. B. A Cryogenic Fluorescence Spectroscopic Study of Uranyl Carbonate, Phosphate and Oxyhydroxide Minerals. *Radiochimica Acta* **2008**, 96 (9–11).
- (17) Wang, Z.; Zachara, J. M.; Gassman, P. L.; Liu, C.; Qafoku, O.; Yantasee, W.; Catalano, J. G. Fluorescence Spectroscopy of U(VI)-Silicates and U(VI)-Contaminated Hanford Sediment. *Geochimica et Cosmochimica Acta* **2005**, 69 (6), 1391–1403.
- (18) Downward, L.; Booth, C. H.; Lukens, W. W.; Bridges, F. A Variation of the F-Test for Determining Statistical Relevance of Particular Parameters in EXAFS Fits. In *AIP Conference Proceedings*; AIP: Stanford, California (USA), 2007; Vol. 882, pp 129–131.
- (19) Stern, E. A. Number of Relevant Independent Points in X-Ray-Absorption Fine-Structure Spectra. *Phys. Rev. B* **1993**, 48 (13), 9825–9827.

References

- (1) Ragnarsdottir, K. V.; Charlet, L. Uranium Behaviour in Natural Environments. In *Environmental Mineralogy: Microbial Interactions, Anthropogenic Influences, Contaminated Land and Waste Management*; Cotter-Howells, J. D., Campbell, L. S., Valsami-Jones, E., Batchelder, M., Eds.; Mineralogical Society of Great Britain and Ireland, 2000; Vol. 9, pp 333–377.
- (2) Danesi, P. R.; Bleise, A.; Burkart, W.; Cabianca, T.; Campbell, M. J.; Makarewicz, M.; Moreno, J.; Tuniz, C.; Hotchkis, M. Isotopic Composition and Origin of Uranium and Plutonium in Selected Soil Samples Collected in Kosovo. *Journal of Environmental Radioactivity* **2003**, 64 (2), 121–131.

- (3) Handley-Sidhu, S.; Keith-Roach, M. J.; Lloyd, J. R.; Vaughan, D. J. A Review of the Environmental Corrosion, Fate and Bioavailability of Munitions Grade Depleted Uranium. *Science of The Total Environment* **2010**, *408* (23), 5690–5700.
- (4) UNEP. *Depleted Uranium in Kosovo, Post-Conflict Environmental Assessment*; United Nations Environment Program: Switzerland., 2001.
- (5) Briner, W. The Toxicity of Depleted Uranium. *IJERPH* **2010**, *7* (1), 303–313.
- (6) Di Lella, L. A.; Frati, L.; Loppi, S.; Protano, G.; Riccobono, F. Environmental Distribution of Uranium and Other Trace Elements at Selected Kosovo Sites. *Chemosphere* **2004**, *56* (9), 861–865.
- (7) Bleise, A.; Danesi, P. R.; Burkart, W. Properties, Use and Health Effects of Depleted Uranium (DU): A General Overview. *Journal of Environmental Radioactivity* **2003**, *64* (2), 93–112.
- (8) Graham, M. C.; Oliver, I. W.; MacKenzie, A. B.; Ellam, R. M.; Farmer, J. G. Mechanisms Controlling Lateral and Vertical Porewater Migration of Depleted Uranium (DU) at Two UK Weapons Testing Sites. *Science of The Total Environment* **2011**, *409* (10), 1854–1866.
- (9) Lind, O. C.; Salbu, B.; Skipperud, L.; Janssens, K.; Jaroszewicz, J.; De Nolf, W. Solid State Speciation and Potential Bioavailability of Depleted Uranium Particles from Kosovo and Kuwait. *Journal of Environmental Radioactivity* **2009**, *100* (4), 301–307.
- (10) Sajih, M.; Livens, F. R.; Alvarez, R.; Morgan, M. Physicochemical Characterisation of Depleted Uranium (DU) Particles at a UK Firing Test Range. *Science of The Total Environment* **2010**, *408* (23), 5990–5996.
- (11) Salbu, B.; Janssens, K.; Lind, O. C.; Proost, K.; Gijssels, L.; Danesi, P. R. Oxidation States of Uranium in Depleted Uranium Particles from Kuwait. *Journal of Environmental Radioactivity* **2005**, *78* (2), 125–135.
- (12) Danesi, P. R.; Markowicz, A.; Chinea-Cano, E.; Burkart, W.; Salbu, B.; Donohue, D.; Ruedenauer, F.; Hedberg, M.; Vogt, S.; Zahradnik, P.; Ciurapinski, A. Depleted Uranium Particles in Selected Kosovo Samples. *Journal of Environmental Radioactivity* **2003**, *64* (2), 143–154.
- (13) Bem, H.; Bou-Rabee, F. Environmental and Health Consequences of Depleted Uranium Use in the 1991 Gulf War. *Environment International* **2004**, *30* (1), 123–134.
- (14) Schimmack, W.; Gerstmann, U.; Oeh, U.; Schultz, W.; Schramel, P. Leaching of Depleted Uranium in Soil as Determined by Column Experiments. *Radiat Environ Biophys* **2005**, *44* (3), 183–191.
- (15) Zachara, J. M.; Long, P. E.; Bargar, J.; Davis, J. A.; Fox, P.; Fredrickson, J. K.; Freshley, M. D.; Konopka, A. E.; Liu, C.; McKinley, J. P.; Rockhold, M. L.; Williams, K. H.; Yabusaki, S. B. Persistence of Uranium Groundwater Plumes: Contrasting Mechanisms at Two DOE Sites in the Groundwater–River Interaction Zone. *Journal of Contaminant Hydrology* **2013**, *147*, 45–72.
- (16) Abdelouas, A.; Lutze, W.; Nuttall, E. Chemical Reactions of Uranium in Ground Water at a Mill Tailings Site. *Journal of Contaminant Hydrology* **1998**, *34* (4), 343–361.
- (17) Brown, P. L.; Guerin, M.; Hankin, S. I.; Lowson, R. T. Uranium and Other Contaminant Migration in Groundwater at a Tropical Australian Uranium Mine. *Journal of Contaminant Hydrology* **1998**, *35* (1–3), 295–303.
- (18) Del Nero, M.; Salah, S.; Miura, T.; Clément, A.; Gauthier-Lafaye, F. Sorption/Desorption Processes of Uranium in Clayey Samples of the Bangombe Natural Reactor Zone, Gabon. *Radiochimica Acta* **1999**, *87* (3–4), 135–150.
- (19) T. Dhomm, R.; J. Evans, G. Evaluation of Uranium and Arsenic Retention by Soil from a Low Level Radioactive Waste Management Site Using Sequential Extraction. *Applied Geochemistry* **1998**, *13* (4), 415–420.
- (20) Gabriel, U.; Gaudet, J.-P.; Spadini, L.; Charlet, L. Reactive Transport of Uranyl in a Goethite Column: An Experimental and Modelling Study. *Chemical Geology* **1998**, *151* (1–4), 107–128.
- (21) Welch, A. H.; Lico, M. S. Factors Controlling As and U in Shallow Ground Water, Southern Carson Desert, Nevada. *Applied Geochemistry* **1998**, *13* (4), 521–539.
- (22) Salbu, B.; Janssens, K.; Lind, O. C.; Proost, K.; Danesi, P. R. Oxidation States of Uranium in DU Particles from Kosovo. *Journal of Environmental Radioactivity* **2003**, *64* (2–3), 167–173.

- (23) Abdelouas, A.; Lu, Y.; Lutze, W.; Nuttall, H. E. Reduction of U^{VI} to U^{IV} by Indigenous Bacteria in Contaminated Ground Water. **1998**, 17.
- (24) Dong, W.; Brooks, S. C. Determination of the Formation Constants of Ternary Complexes of Uranyl and Carbonate with Alkaline Earth Metals (Mg²⁺, Ca²⁺, Sr²⁺, and Ba²⁺) Using Anion Exchange Method. *Environ. Sci. Technol.* **2006**, 40 (15), 4689–4695.
- (25) Meleshyn, A.; Azeroual, M.; Reeck, T.; Houben, G.; Riebe, B.; Bunnenberg, C. Influence of (Calcium–)Uranyl–Carbonate Complexation on U(VI) Sorption on Ca- and Na-Bentonites. *Environ. Sci. Technol.* **2009**, 43 (13), 4896–4901.
- (26) Zeh, P.; Czerwinski, K. R.; Kim, J. I. Speciation of Uranium in Gorleben Groundwaters. *Radiochimica Acta* **1997**, 76 (1–2), 37–44.
- (27) Lenhart, J. J.; Cabaniss, S. E.; MacCarthy, P.; Honeyman, B. D. Uranium(VI) Complexation with Citric, Humic and Fulvic Acids. *Radiochimica Acta* **2000**, 88 (6), 345–354.
- (28) Crançon, P.; van der Lee, J. Speciation and Mobility of Uranium(VI) in Humic-Containing Soils. *Radiochimica Acta* **2003**, 91 (11).
- (29) Bryan, N. D.; Abrahamsen, L.; Evans, N.; Warwick, P.; Buckau, G.; Weng, L.; Van Riemsdijk, W. H. The Effects of Humic Substances on the Transport of Radionuclides: Recent Improvements in the Prediction of Behaviour and the Understanding of Mechanisms. *Applied Geochemistry* **2012**, 27 (2), 378–389.
- (30) Moulin, V.; Moulin, C. Fate of Actinides in the Presence of Humic Substances under Conditions Relevant to Nuclear Waste Disposal. *Applied Geochemistry* **1995**, 10, 573–580.
- (31) Reiller, P. E.; Buckau, G. Impacts of Humic Substances on the Geochemical Behaviour of Radionuclides. In *Radionuclide Behaviour in the Natural Environment*; Elsevier, 2012; pp 103–160.
- (32) Graham, M. C.; Oliver, I. W.; MacKenzie, A. B.; Ellam, R. M.; Farmer, J. G. An Integrated Colloid Fractionation Approach Applied to the Characterisation of Porewater Uranium–Humic Interactions at a Depleted Uranium Contaminated Site. *Science of The Total Environment* **2008**, 404 (1), 207–217.
- (33) Chen, J. P.; Yiacoumi, S. Modeling of Depleted Uranium Transport in Subsurface Systems.
- (34) Davis, J. A.; Curtis, G. P.; Wilkins, M. J.; Kohler, M.; Fox, P.; Naftz, D. L.; Lloyd, J. R. Processes Affecting Transport of Uranium in a Suboxic Aquifer. *Physics and Chemistry of the Earth, Parts A/B/C* **2006**, 31 (10–14), 548–555.
- (35) Senko, J. M.; Istok, J. D.; Suflita, J. M.; Krumholz, L. R. In - Situ Evidence for Uranium Immobilization and Remobilization. *Environ. Sci. Technol.* **2002**, 36 (7), 1491–1496.
- (36) Artinger, R.; Rabung, T.; Kim, J. I.; Sachs, S.; Schmeide, K.; Heise, K. H.; Bernhard, G.; Nitsche, H. Humic Colloid-Borne Migration of Uranium in Sand Columns. *Journal of Contaminant Hydrology* **2002**, 58 (1–2), 1–12.
- (37) Crançon, P.; Pili, E.; Charlet, L. Uranium Facilitated Transport by Water-Dispersible Colloids in Field and Soil Columns. *Science of The Total Environment* **2010**, 408 (9), 2118–2128.
- (38) Mibus, J.; Sachs, S.; Pfingsten, W.; Nebelung, C.; Bernhard, G. Migration of Uranium(IV)/(VI) in the Presence of Humic Acids in Quartz Sand: A Laboratory Column Study. *Journal of Contaminant Hydrology* **2007**, 89 (3–4), 199–217.
- (39) Oliver, I. W.; Graham, M. C.; MacKenzie, A. B.; Ellam, R. M.; Farmer, J. G. Depleted Uranium Mobility Across a Weapons Testing Site: Isotopic Investigation of Porewater, Earthworms, and Soils. *Environ. Sci. Technol.* **2008**, 42 (24), 9158–9164.
- (40) Andersson, P. S.; Porcelli, D.; Wasserburg, G. J.; Ingri, J. Particle Transport of ²³⁴U–²³⁸U in the Kalix River and in the Baltic Sea.
- (41) Franke, K.; Röbller, D.; Gottschalch, U.; Kupsch, H. Mobilization and Retardation of Uranium DOC Species at Three Mine Piles in Schlema/Alberoda, Saxony, Germany. *Isotopes in Environmental and Health Studies* **2000**, 36 (3), 223–239.
- (42) Harguindeguy, S.; Crançon, P.; Potin Gautier, M.; Pointurier, F.; Lespes, G. Colloidal Mobilization from Soil and Transport of Uranium in (Sub)-Surface Waters. *Environ Sci Pollut Res* **2019**, 26 (6), 5294–5304.
- (43) Harguindeguy, S.; Crançon, P.; Pointurier, F.; Potin-Gautier, M.; Lespes, G. Isotopic Investigation of the Colloidal Mobility of Depleted Uranium in a Podzolic Soil. *Chemosphere* **2014**, 103, 343–348.

- (44) Ho, C. H.; Miller, N. H. Adsorption of Uranyl Species from Bicarbonate Solution onto Hematite Particles. *Journal of Colloid and Interface Science* **1986**, *110* (1), 165–171.
- (45) Crançon, P.; Mangeret, A.; De Windt, L. Assessing Migration of Uranium through Chalk Substrate: Field Study and Reactive Transport Modelling. *IJEPR* **2012**.
- (46) Stewart, B. D.; Mayes, M. A.; Fendorf, S. Impact of Uranyl–Calcium–Carbonato Complexes on Uranium(VI) Adsorption to Synthetic and Natural Sediments. *Environ. Sci. Technol.* **2010**, *44* (3), 928–934.
- (47) Prat, O.; Vercoouter, T.; Ansoborlo, E.; Fichet, P.; Perret, P.; Kurttio, P.; Salonen, L. Uranium Speciation in Drinking Water from Drilled Wells in Southern Finland and Its Potential Links to Health Effects. *Environ. Sci. Technol.* **2009**, *43* (10), 3941–3946.
- (48) Hamilton, E. I. Depleted Uranium ž DU/ : A Holistic Consideration of DU and Related Matters. **2001**.
- (49) Sansone, U.; Stellato, L.; Jia, G.; Rosamilia, S.; Gaudino, S.; Barbizzi, S.; Belli, M. LEVELS OF DEPLETED URANIUM IN KOSOVO SOILS.
- (50) Oliver, I. W.; MacKenzie, A. B.; Ellam, R. M.; Graham, M. C.; Farmer, J. G. Determining the Extent of Depleted Uranium Contamination in Soils at a Weapons Test Site: An Isotopic Investigation. *Geochimica et Cosmochimica Acta* **2006**, *18* (70), A457.
- (51) Oliver, I. W.; Graham, M. C.; MacKenzie, A. B.; Ellam, R. M.; Farmer, J. G. Assessing Depleted Uranium (DU) Contamination of Soil, Plants and Earthworms at UK Weapons Testing Sites. *J. Environ. Monit.* **2007**, *9* (7), 740.
- (52) Toque, C.; Milodowski, A. E.; Baker, A. C. The Corrosion of Depleted Uranium in Terrestrial and Marine Environments. *Journal of Environmental Radioactivity* **2014**, *128*, 97–105.
- (53) Papastefanou, C. DEPLETED URANIUM IN MILITARY CONFLICTS AND THE IMPACT ON THE ENVIRONMENT: *Health Physics* **2002**, *83* (2), 280–282.
- (54) Radenković, M. B.; Cupać, S. A.; Joksić, J. D.; Todorović, D. J. Depleted Uranium Mobility and Fractionation in Contaminated Soil (Southern Serbia). *Environ Sci Pollut Res* **2008**, *15* (1), 61–67.
- (55) Sansone, U.; Roberto Danesi, P.; Barbizzi, S.; Belli, M.; Campbell, M.; Gaudino, S.; Jia, G.; Ocone, R.; Pati, A.; Rosamilia, S.; Stellato, L. Radioecological Survey at Selected Sites Hit by Depleted Uranium Ammunitions during the 1999 Kosovo Conflict. *Science of The Total Environment* **2001**, *281* (1–3), 23–35.
- (56) Lind, O. C.; Salbu, B.; Janssens, K.; Proost, K.; Danesi, P. R. Characterisation of DU Particles from Kosovo and Kuwait. *Radioactive Particles in the Environment* **2009**, 57–67.
- (57) Oliver, I. W.; Graham, M. C.; MacKenzie, A. B.; Ellam, R. M.; Farmer, J. G. Distribution and Partitioning of Depleted Uranium (DU) in Soils at Weapons Test Ranges – Investigations Combining the BCR Extraction Scheme and Isotopic Analysis. *Chemosphere* **2008**, *72* (6), 932–939.
- (58) Haschke, J. M. Corrosion of Uranium in Air and Water Vapor: Consequences for Environmental Dispersal. *Journal of Alloys and Compounds* **1998**, *278* (1–2), 149–160.
- (59) Cachoïr, C.; Gallien, J. P.; Trocellier, P. Chemical Durability of Uranium Dioxide Stored in Geologic Medium : Uranium Remobilisation. *Annales de Chimie-Science des Matériaux* **1996**, *21* (8), 567–592.
- (60) McEachern, R. J.; Taylor, P. A Review of the Oxidation of Uranium Dioxide at Temperatures below 400°C. *Journal of Nuclear Materials* **1998**, *254* (2–3), 87–121.
- (61) Schimmack, W.; Gerstmann, U.; Schultz, W.; Geipel, G. Long-Term Corrosion and Leaching of Depleted Uranium (DU) in Soil. *Radiat Environ Biophys* **2007**, *46* (3), 221–227.
- (62) Handley-Sidhu, S.; Bryan, N. D.; Worsfold, P. J.; Vaughan, D. J.; Livens, F. R.; Keith-Roach, M. J. Corrosion and Transport of Depleted Uranium in Sand-Rich Environments. *Chemosphere* **2009**, *77* (10), 1434–1439.
- (63) Finch, R. J.; Ewing, R. C. The Corrosion of Uraninite under Oxidizing Conditions. *Journal of Nuclear Materials* **1992**, *190*, 133–156.
- (64) Gorman-Lewis, D.; Burns, P. C.; Fein, J. B. Review of Uranyl Mineral Solubility Measurements. *The Journal of Chemical Thermodynamics* **2008**, *40* (3), 335–352.
- (65) Bower, W. R.; Morris, K.; Livens, F. R.; Mosselmans, J. F. W.; Fallon, C. M.; Fuller, A. J.; Natrajan, L.; Boothman, C.; Lloyd, J. R.; Utsunomiya, S.; Grolimund, D.; Ferreira Sanchez, D.;

- Jilbert, T.; Parker, J.; Neill, T. S.; Law, G. T. W. Metaschoepite Dissolution in Sediment Column Systems—Implications for Uranium Speciation and Transport. *Environ. Sci. Technol.* **2019**, *53* (16), 9915–9925.
- (66) Hubert, A.; Bourdon, B.; Pili, E.; Meynadier, L. Transport of Radionuclides in an Unconfined Chalk Aquifer Inferred from U-Series Disequilibria. *Geochimica et Cosmochimica Acta* **2006**, *70* (22), 5437–5454.
- (67) Bourdon, B.; Bureau, S.; Andersen, M. B.; Pili, E.; Hubert, A. Weathering Rates from Top to Bottom in a Carbonate Environment. *Chemical Geology* **2009**, *258* (3–4), 275–287.
- (68) Renard, F.; Jeannée, N. Estimating Transmissivity Fields and Their Influence on Flow and Transport: The Case of Champagne Mounts. *Water Resour. Res.* **2008**, *44* (11), 1-12 (W11414).
- (69) Gillon, M.; Crançon, P.; Aupiais, J. Modelling the Baseline Geochemistry of Groundwater in a Chalk Aquifer Considering Solid Solutions for Carbonate Phases. *Applied Geochemistry* **2010**, *25* (10), 1564–1574.
- (70) Gillon, M.; Renard, F.; Crançon, P.; Aupiais, J. Kinetics of Incongruent Dissolution of Carbonates in a Chalk Aquifer Using Reverse Flow Modelling. *Journal of Hydrology* **2012**, *420–421*, 329–339.
- (71) Mangeret, A.; De Windt, L.; Crançon, P. Reactive Transport Modelling of Groundwater Chemistry in a Chalk Aquifer at the Watershed Scale. *Journal of Contaminant Hydrology* **2012**, *138–139*, 60–74.
- (72) Claveranne-Lamolère, C.; Aupiais, J.; Lespes, G.; Frayret, J.; Pili, E.; Pointurier, F.; Potin-Gautier, M. Investigation of Uranium–Colloid Interactions in Soil by Dual Field-Flow Fractionation/Capillary Electrophoresis Hyphenated with Inductively Coupled Plasma-Mass Spectrometry. *Talanta* **2011**, *85* (5), 2504–2510.
- (73) Claveranne-Lamolère, C.; Lespes, G.; Dubascoux, S.; Aupiais, J.; Pointurier, F.; Potin-Gautier, M. Colloidal Transport of Uranium in Soil: Size Fractionation and Characterization by Field-Flow Fractionation–Multi-Detection. *Journal of Chromatography A* **2009**, *1216* (52), 9113–9119.
- (74) Cao, F.; Jaunat, J.; Vergnaud-Ayraud, V.; Devau, N.; Labasque, T.; Guillou, A.; Guillaneuf, A.; Hubert, J.; Aquilina, L.; Ollivier, P. Heterogeneous Behaviour of Unconfined Chalk Aquifers Infer from Combination of Groundwater Residence Time, Hydrochemistry and Hydrodynamic Tools. *Journal of Hydrology* **2020**, *581*, 124433.
- (75) Cao, F.; Sturchio, N. C.; Ollivier, P.; Devau, N.; Heraty, L. J.; Jaunat, J. Sources and Behavior of Perchlorate in a Shallow Chalk Aquifer under Military (World War I) and Agricultural Influences. *Journal of Hazardous Materials* **2020**, *398*, 1-14 (123072).
- (76) Knechtenhofer, L. A.; Xifra, I. O.; Scheinost, A. C.; Flühler, H.; Kretzschmar, R. Fate of Heavy Metals in a Strongly Acidic Shooting- range Soil: Small- scale Metal Distribution and Its Relation to Preferential Water Flow. *Journal of Plant Nutrition and Soil Science* **2003**, *166* (1), 84–92.
- (77) Bruno, J.; Sandino, A. The Solubility of Amorphous and Crystalline Schoepite in Neutral to Alkaline Aqueous Solutions. *MRS Proc.* **1988**, *127*, 871–878.
- (78) Vdović, N. Electrokinetic Behaviour of Calcite—the Relationship with Other Calcite Properties. *Chemical Geology* **2001**, *177* (3–4), 241–248.
- (79) Kim, J. I.; Buckau, G.; Li, G. H.; Duschner, H.; Psarros, N. Characterization of Humic and Fulvic Acids from Gorleben Groundwater. *Fresenius J Anal Chem* **1990**, *338* (3), 245–252.
- (80) Ayawei, N.; Ebelegi, A. N.; Wankasi, D. Modelling and Interpretation of Adsorption Isotherms. *Journal of Chemistry* **2017**, *2017*, 1–11.
- (81) Boparai, H. K.; Joseph, M.; O’Carroll, D. M. Kinetics and Thermodynamics of Cadmium Ion Removal by Adsorption onto Nano Zerovalent Iron Particles. *Journal of Hazardous Materials* **2011**, *186* (1), 458–465.
- (82) Sparks, D. L. Sorption Phenomena on Soils. In *Environmental Soil Chemistry*; Academic Press: Burlington, 2003; pp 133–186.
- (83) Azizian, S.; Eris, S. Chapter 6 - Adsorption Isotherms and Kinetic. In *Interface Science and Technology*; Elsevier, 2021; pp 445–509.

- (84) Sitaud, B.; Solari, P. L.; Schlutig, S.; Llorens, I.; Hermange, H. Characterization of Radioactive Materials Using the MARS Beamline at the Synchrotron SOLEIL. *Journal of Nuclear Materials* **2012**, *425* (1), 238–243.
- (85) Llorens, I.; Solari, P. L.; Sitaud, B.; Bes, R.; Cammelli, S.; Hermange, H.; Othmane, G.; Safi, S.; Moisy, P.; Wahu, S.; Bresson, C.; Schlegel, M. L.; Menut, D.; Bechade, J.-L.; Martin, P.; Hazemann, J.-L.; Proux, O.; Auwer, C. D. X-Ray Absorption Spectroscopy Investigations on Radioactive Matter Using MARS Beamline at SOLEIL Synchrotron. *Radiochimica Acta* **2014**, *102* (11), 957–972.
- (86) Ravel, B.; Newville, M. ATHENA, ARTEMIS, HEPHAESTUS: Data Analysis for X-Ray Absorption Spectroscopy Using IFEFFIT. *Journal of Synchrotron Radiation* **2005**, *12* (4), 537–541.
- (87) Dong, W.; Ball, W. P.; Liu, C.; Wang, Z.; Stone, A. T.; Bai, J.; Zachara, J. M. Influence of Calcite and Dissolved Calcium on Uranium(VI) Sorption to a Hanford Subsurface Sediment. *Environ. Sci. Technol.* **2005**, *39* (20), 7949–7955.
- (88) Geipel, G.; Reich, T.; Brendler, V.; Bernhard, G.; Nitsche, H. Laser and X-Ray Spectroscopic Studies of Uranium-Calcite Interface Phenomena. *Journal of Nuclear Materials* **1997**, *248*, 408–411.
- (89) Niu, Z.; Wei, X.; Qiang, S.; Wu, H.; Pan, D.; Wu, W.; Fan, Q. Spectroscopic Studies on U(VI) Incorporation into CaCO₃: Effects of Aging Time and U(VI) Concentration. *Chemosphere* **2019**, *220*, 1100–1107.
- (90) Elzinga, E. J.; Tait, C. D.; Reeder, R. J.; Rector, K. D.; Donohoe, R. J.; Morris, D. E. Spectroscopic Investigation of U(VI) Sorption at the Calcite-Water Interface. *Geochimica et Cosmochimica Acta* **2004**, *68* (11), 2437–2448.
- (91) Géhin, A.; Markelov, I.; Crançon, P.; Charlet, L. Thermodynamic and Kinetic Properties of U(VI) Sorption on Chalk Substrates, 2016.
- (92) Waite, T. D.; Davis, J. A.; Fenton, B. R.; Payne, T. E. Approaches to Modelling Uranium(VI) Adsorption on Natural Mineral Assemblages. *Radiochimica Acta* **2000**, *88* (9–11), 687–694.
- (93) Catalano, J. G.; Brown, G. E. Uranyl Adsorption onto Montmorillonite: Evaluation of Binding Sites and Carbonate Complexation. *Geochimica et Cosmochimica Acta* **2005**, *69* (12), 2995–3005.
- (94) Beneš, P.; Kratzer, K.; Vlčková, Š.; Šebestová, E. Adsorption of Uranium on Clay and the Effect of Humic Substances. *Radiochimica Acta* **1998**, *82* (s1), 367–374.
- (95) Ho, C. H.; Miller, N. H. Effect of Humic Acid on Uranium Uptake by Hematite Particles. *Journal of Colloid and Interface Science* **1985**, *106* (2), 281–288.
- (96) Lenhart, J. J.; Honeyman, B. D. Uranium(VI) Sorption to Hematite in the Presence of Humic Acid. *Geochimica et Cosmochimica Acta* **1999**, *63* (19–20), 2891–2901.
- (97) Payne, T. E.; Davis, J. A.; Waite, T. D. Uranium Adsorption on Ferrihydrite - Effects of Phosphate and Humic Acid. *Radiochimica Acta* **1996**, *74* (s1), 239–244.
- (98) Schmeide, K.; Pompe, S.; Bubner, M.; Heise, K. H.; Bernhard, G.; Nitsche, H. Uranium(VI) Sorption onto Phyllite and Selected Minerals in the Presence of Humic Acid. *Radiochimica Acta* **2000**, *88* (9–11), 723–728.
- (99) Wei, M.; Liao, J.; Liu, N.; Zhang, D.; Kang, H.; Yang, Y.; Yang, Y.; Jin, J. Interaction between Uranium and Humic Acid (1): Adsorption Behaviors of U(VI) in Soil Humic Acids. *Nuclear Science and Techniques* **2007**, *18* (5), 287–293.
- (100) Luo, W.; Gu, B. Dissolution and Mobilization of Uranium in a Reduced Sediment by Natural Humic Substances under Anaerobic Conditions. *Environ. Sci. Technol.* **2009**, *43* (1), 152–156.
- (101) Sylwester, E. R.; Hudson, E. A.; Allen, P. G. The Structure of Uranium (VI) Sorption Complexes on Silica, Alumina, and Montmorillonite. *Geochimica et Cosmochimica Acta* **2000**, *64* (14), 2431–2438.
- (102) Wang, Z.; Zachara, J. M.; Liu, C.; Gassman, P. L.; Felmy, A. R.; Clark, S. B. A Cryogenic Fluorescence Spectroscopic Study of Uranyl Carbonate, Phosphate and Oxyhydroxide Minerals. *Radiochimica Acta* **2008**, *96* (9–11).
- (103) Finch, R. J.; Cooper, M. A.; Hawthorne, F. C. The Crystal Structure of Schoepite [(UO₂)₈O₂(OH)₁₂](H₂O)₁₂. *The Canadian Mineralogist* **1996**, *34*, 1071–1088.

- (104) Allen, P. G.; Shuh, D. K.; Bucher, J. J.; Edelstein, N. M.; Palmer, C. E. A.; Silva, R. J.; Nguyen, S. N.; Marquez, L. N.; Hudson, E. A. Determinations of Uranium Structures by EXAFS: Schoepite and Other U(VI) Oxide Precipitates. *Radiochimica Acta* **1996**, *75* (1).
- (105) Denecke, M. A.; Pompe, S.; Reich, T.; Moll, H.; Bubner, M.; Heise, K. H.; Nicolai, R.; Nitsche, H. Measurements of the Structural Parameters for the Interaction of Uranium(VI) with Natural and Synthetic Humic Acids Using EXAFS. *Radiochimica Acta* **1997**, *79* (3), 151–160.
- (106) Denecke, M. A.; Reich, T.; Bubner, M.; Pompe, S.; Heise, K. H.; Nitsche, H.; Allen, P. G.; Bucher, J. J.; Edelstein, N. M.; Shuh, D. K. Determination of Structural Parameters of Uranyl Ions Complexed with Organic Acids Using EXAFS. *Journal of Alloys and Compounds* **1998**, *271–273*, 123–127.
- (107) Steudtner, R.; Müller, K.; Schmeide, K.; Sachs, S.; Bernhard, G. Binary and Ternary Uranium(vi) Humate Complexes Studied by Attenuated Total Reflection Fourier-Transform Infrared Spectroscopy. *Dalton Trans.* **2011**, *40* (44), 11920.
- (108) Huang, Z.; Li, Z.; Zheng, L.; Zhou, L.; Chai, Z.; Wang, X.; Shi, W. Interaction Mechanism of Uranium(VI) with Three-Dimensional Graphene Oxide-Chitosan Composite: Insights from Batch Experiments, IR, XPS, and EXAFS Spectroscopy. *Chemical Engineering Journal* **2017**, *328*, 1066–1074.
- (109) Kelly, S. D.; Kemner, K. M.; Brooks, S. C. X-Ray Absorption Spectroscopy Identifies Calcium-Uranyl-Carbonate Complexes at Environmental Concentrations. *Geochimica et Cosmochimica Acta* **2007**, *71* (4), 821–834.
- (110) Wang, Z.; Zachara, J. M.; McKinley, J. P.; Smith, S. C. Cryogenic Laser Induced U(VI) Fluorescence Studies of a U(VI) Substituted Natural Calcite: Implications to U(VI) Speciation in Contaminated Hanford Sediments. *Environ. Sci. Technol.* **2005**, *39* (8), 2651–2659.
- (111) Wang, Z.; Zachara, J. M.; Gassman, P. L.; Liu, C.; Qafoku, O.; Yantasee, W.; Catalano, J. G. Fluorescence Spectroscopy of U(VI)-Silicates and U(VI)-Contaminated Hanford Sediment. *Geochimica et Cosmochimica Acta* **2005**, *69* (6), 1391–1403.
- (112) Wang, Z.; Zachara, J. M.; Yantasee, W.; Gassman, P. L.; Liu, C.; Joly, A. G. Cryogenic Laser Induced Fluorescence Characterization of U(VI) in Hanford Vadose Zone Pore Waters. *Environ. Sci. Technol.* **2004**, *38* (21), 5591–5597.
- (113) Finch, R. J.; Hawthorne, F. C.; Ewing, R. C. Structural Relations among Schoepite, Metaschoepite, and “Dehydrated Schoepite.” *The Canadian Mineralogist* **1998**, *36*, 831–845.
- (114) Killough, G. G.; Rope, S. K.; Shleien, B.; Voillequé, P. G. Nonlinear Estimation of Weathering Rate Parameters for Uranium in Surface Soil near a Nuclear Facility. *Journal of Environmental Radioactivity* **1999**, *45* (2), 95–118.
- (115) McGillivray, G. W.; Geeson, D. A.; Greenwood, R. C. Studies of the Kinetics and Mechanism of the Oxidation of Uranium by Dry and Moist Air A Model for Determining the Oxidation Rate over a Wide Range of Temperatures and Water Vapour Pressures. *Journal of Nuclear Materials* **1994**, *208* (1–2), 81–97.
- (116) Török, S.; Osán, J.; Vincze, L.; Kurunczi, S.; Tamborini, G.; Betti, M. Characterization and Speciation of Depleted Uranium in Individual Soil Particles Using Microanalytical Methods. *Spectrochimica Acta Part B: Atomic Spectroscopy* **2004**, *59* (5), 689–699.
- (117) Ivanov, Y. Ivanov, Y. (2009). Migration of Fuel Particles of CHNPP Fallout and Leached Radionuclides in Soils and Soil-to-Plant System. In *Radioactive Particles in the Environment* (Pp. 123-137). Springer Netherlands. In *Radioactive Particles in the Environment*; Springer Netherlands., 2009; pp 123–137.
- (118) Victorova, N. N.; Demchuk, V. V.; Ganga, E. V.; Tretyakova, S. P.; Golovchenko, A. N. Nondestructive Control of Chernobyl Hot Particles Behavior and Migration of Radionuclides in Soil-Plant System. *Nuclear Tracks and Radiation Measurements* **1993**, *22* (1–4), 885–888.
- (119) Kliashorin, A. L.; Shcheglov, A. I.; Tikhomirov, F. A. Vertical Migration of Radionuclides from the Chernobyl Fallout in Different Types of Soil., In *International Conference On Environmental Pollution, The Proceedings: Vol.1 and 2.*; 1996; pp 702–709.
- (120) Tejada, I. G.; Sibille, L.; Chareyre, B.; Vincens, E. Numerical Modeling of Particle Migration in Granular Soils. In *Scour and Erosion: Proceedings of the 8th International Conference on Scour and Erosion*; CRC Press: Oxford, UK, 2016; p 139.

- (121) Qin, Z.; Lijun, S.; Zhenyu, L.; Shihao, Y. Study of Seepage in Wide-Grading Soils with Particles Migration. *Chinese J Rock Soil Mech* **2021**, *42* (1), 125–134.
- (122) Whicker, R. D.; Ibrahim, S. A. Vertical Migration of ¹³⁴Cs Bearing Soil Particles in Arid Soils: Implications for Plutonium Redistribution. *Journal of Environmental Radioactivity* **2006**, *88* (2), 171–188.
- (123) Tanaka, T.; Ohnuki, T. Colloidal Migration Behavior of Radionuclides Sorbed on Mobile Fine Soil Particles through a Sand Layer. *Journal of Nuclear Science and Technology* **1996**, *33* (1), 62–68.
- (124) Ogawa, H.; Takebe, S.; Yamamoto, T. Evaluation of Migration of Cesium-137 Adsorbed on Fine Soil Particles through Natural Aerated Soil Layer. *Journal of Nuclear Science and Technology* **1991**, *28* (3), 248–254.
- (125) Reeder, R. J.; Elzinga, E. J.; Tait, C. D.; Rector, K. D.; Donohoe, R. J.; Morris, D. E. Site-Specific Incorporation of Uranyl Carbonate Species at the Calcite Surface. *Geochimica et Cosmochimica Acta* **2004**, *68* (23), 4799–4808.
- (126) Reeder, R. J.; Nugent, M.; Lambie, G. M.; Tait, C. D.; Morris, D. E. Uranyl Incorporation into Calcite and Aragonite: XAFS and Luminescence Studies. *Environ. Sci. Technol.* **2000**, *34* (4), 638–644.
- (127) Doudou, S.; Vaughan, D. J.; Livens, F. R.; Burton, N. A. Atomistic Simulations of Calcium Uranyl(VI) Carbonate Adsorption on Calcite and Stepped-Calcite Surfaces. *Environ. Sci. Technol.* **2012**, *46* (14), 7587–7594.